https://doi.org/10.17221/24/2026-JFS

Ozone phytotoxicity in the Czech Republic: Insights from exposure- and flux-based metrics and visible foliar injury in European beech and Norway spruce

Leona Vlasáková[1], *Radek Novotný*[2], *Nina Benešová*[1], *Vít Šrámek*[2], *Václav Buriánek*[2]

[1]*Air Quality Division, Czech Hydrometeorological Institute, Prague, Czech Republic*
[2]*Forestry and Game Management Research Institute, Prague, Czech Republic*

**Corresponding author: leona.vlasakova@chmi.cz*

Citation: Vlasáková L., Novotný R., Benešová N., Šrámek V., Buriánek V. (2026): Ozone phytotoxicity in the Czech Republic: Insights from exposure- and flux-based metrics and visible foliar injury in European beech and Norway spruce. J. For. Sci., 72: 213–235.

Abstract: This study evaluated the phytotoxic potential of ground-level ozone (O_3) on native forest tree species at eight intensive forest monitoring plots in the Czech Republic. O_3 risk was assessed using the exposure-based AOT40F (accumulated O_3 concentration above 40 ppb for forest protection) and the flux-based POD_1 (phytotoxic ozone dose above a flux threshold of 1 nmol O_3 $m^{-2}{\cdot}s^{-1}$ per leaf area) indices, together with data on visible foliar O_3 injury. The analysis was based on data from the 2021–2023 vegetation seasons. AOT40F exceeded the critical level of 5 ppm·h at all plots. The critical levels of POD_1 (5.2 mmol·m^{-2} for *Fagus sylvatica* and 9.2 mmol·m^{-2} for *Picea abies*) were exceeded at all sites in all seasons, except for one plot in 2022. Exceedance of POD_1 generally occurred earlier than that of AOT40F for *F. sylvatica*, while for *P. abies* it occurred later in the season. POD_1 showed a significant positive relationship with altitude, but AOT40F did not. Air temperature, soil moisture, and the O_3 concentration were identified as the main predictors of stomatal O_3 flux. Visible O_3 injury was absent in *P. abies* and limited in *F. sylvatica*, with a weak relationship to the O_3 metrics. The results emphasise the greater relevance of flux-based approaches for O_3 risk assessment and indicate that visible foliar O_3 injury alone provides only a limited indicator of O_3 impacts under Czech conditions.

Keywords: AOT40; ground-level ozone; critical level; O_3 injury; phytotoxic ozone dose

Ground-level (tropospheric) ozone (O_3) is a key secondary photochemical pollutant formed through complex chain reactions of its precursors, originating from both natural and anthropogenic sources (Fowler et al. 2008; Monks et al. 2015; Anav et al. 2016). O_3 concentrations exhibit significant temporal and spatial variability, which depends on numerous factors, including geographic location, altitude, season, and synoptic conditions. The ideal conditions for the photochemical forma-

Supported by the ARAMIS project – Integrated System of Research, Evaluation and Control of Air Quality, and co-founded with the state support of the Technology Agency of the Czech Republic under the Environment for Life program (Grant No. SS02030031). Within the article, ICP Forests data was used and evaluated with the institutional support of the Ministry of Agriculture (No. MZE-RO0123).

https://doi.org/10.17221/24/2026-JFS

tion of O_3 are generally considered to include high air temperature, high solar radiation intensity, low wind speed, low relative humidity, and the absence of atmospheric precipitation (Finlayson-Pitts, Pitts 2000).

Due to its high reactivity, O_3 is widely recognised as the most damaging common air pollutant to vegetation, exerting adverse effects on crop productivity and forest health (Ashmore 2005; Paoletti, Manning 2007; Mills et al. 2011; Fares et al. 2018). O_3-induced injury occurs at multiple biological levels, from cellular and physiological processes to whole-plant performance and ecosystem-level responses (Fuhrer 2002; Ainsworth 2016; Mills et al. 2018). Plants subjected to O_3 stress often exhibit increased sensitivity to additional abiotic and biotic stressors (Langebartels et al. 1998; Jones et al. 2004). Additionally, elevated O_3 concentrations threaten terrestrial biodiversity and ecosystem services (Mills et al. 2018; Agathokleous et al. 2020; Reif et al. 2023).

During O_3 exposure, oxidative stress triggers an initial oxidative burst in leaf tissues, leading to damage of cell membranes, hypersensitive-like cell response or accelerated cell senescence, as well as structural modifications of the cell wall, which may manifest externally as visible foliar injury (Pell et al. 1997; Vollenweider et al. 2003). Visible foliar O_3 injury is widely regarded as the earliest indicator of a phytotoxic O_3 dose and provides a reliable means of assessing O_3 impacts over short time periods under field conditions (Bergmann et al. 1999; Schaub et al. 2013). Importantly, these symptoms are considered specific to O_3 exposure and are not confounded by other co-occurring stress factors, which makes them particularly valuable in forest monitoring programmes (Sicard et al. 2016a; Paoletti et al. 2019). Recent evidence indicates that trees exhibiting visible O_3 injury tend to show greater crown defoliation and reduced annual radial growth compared to asymptomatic individuals (Paoletti et al. 2019). Moreover, evidence from free-air controlled O_3 exposure experiments demonstrates a clear relationship between the occurrence of visible foliar O_3 injury and reductions in total tree biomass (Paoletti et al. 2022). Visible foliar O_3 injury, systematically recorded in large-scale forest surveys, represents a good forest health indicator of tree responses to ambient O_3 under field conditions. This type of injury provides a rapid and cost-effective signal of O_3 stress, enables early identification of potentially affected stands, and serves as a first-step tool for assessing O_3-related forest health risks, thereby guiding the need for more detailed research (Coulston et al. 2003; Paoletti et al. 2019; Sicard et al. 2021).

Nevertheless, species, genotypes, canopy position, nutrient status, stomatal regulation, antioxidant capacity and phenology can modulate symptom expression, and identical O_3 exposures may not lead to comparable visible foliar O_3 injury across sites or species (Manning, Godzik 2004; Emberson et al. 2000; Dumont et al. 2013; Sicard et al. 2016b; Agathokleous et al. 2019; Bičárová et al. 2020; Lukasová et al. 2025). Coniferous and broadleaved tree species namely differ in a range of structural and functional traits, including leaf anatomy (Huttunen, Manninen 2013; Zhang et al. 2020), stomatal conductance (Medlyn et al. 2001), leaf or needle longevity, metabolic rate (Withington et al. 2006), or antioxidant capacity (Burkey et al. 2000). Consequently, broadleaved species may be more sensitive to the effects of O_3 than coniferous species, at least in the short term (Skärby et al. 1998; Karlsson et al. 2025; Bergmann et al. 2017; Marra et al. 2025). Recent studies from mountainous regions of Central Europe highlight that O_3 sensitivity among coniferous species can vary substantially depending on species-specific traits and local environmental conditions (Bičárová et al. 2020; Lukasová et al. 2025).

Currently, European Directives 2008/50/EC (EC 2008) and 2024/2881/EU (EU 2024) use the accumulated O_3 exposure over a threshold of 40 ppb (AOT40) as an indicator to protect vegetation against the adverse impacts of O_3. In the Czech Republic, AOT40 values across forested areas exceeded the critical level (*CL*) for forest protection throughout the period 2000–2015, with only a minor exception in 2009, indicating persistent exceedances over the entire study period (Hůnová et al. 2019). However, this concentration-based approach does not reflect the actual dose of O_3 absorbed by plants, as it does not account for stomatal uptake and factors controlling stomatal conductance (Anav et al. 2016). As a result, AOT40 may overestimate or underestimate the impacts of O_3, depending on the prevailing meteorological conditions and the vegetation physiological status.

Considering the limitations of concentration-based metrics, a growing body of evidence has demonstrated that the impacts of O_3 on vegetation

https://doi.org/10.17221/24/2026-JFS

are more related to the stomatal O_3 flux absorbed through the stomata than to O_3 concentrations alone, as only O_3 molecules entering the leaf interior are phytotoxic (Musselman, Massman 1999; Nussbaum et al. 2003; Matyssek et al. 2007; Fares et al. 2010). The stomatal flux framework accounts for key drivers of stomatal conductance, including phenology, air temperature, soil moisture, vapour pressure deficit, and solar radiation (Emberson et al. 2000). As a result, flux-based metrics explain why high O_3 concentrations may not lead to injury when stomata are closed under unfavourable conditions (Paoletti 2006; Ronan et al. 2020), while relatively low concentrations may still cause damage when stomata are open under favourable environmental conditions (Matyssek et al. 2007; Karlsson et al. 2017).

Reflecting this scientific consensus, *POD*-based *CL*s have been adopted within the Convention on Long-Range Transboundary Air Pollution (CLRTAP) as a more biologically meaningful basis for O_3 risk assessment, and a flux-based approach is being considered as the basis for future forest protection standards (Mills et al. 2011; CLRTAP 2017). Current European policy frameworks already recommend ecosystem monitoring based on O_3 fluxes and visible foliar O_3 injury (EU 2016, 2019), supporting a transition towards a biologically sound, stomatal flux-based standard – the phytotoxic O_3 dose over a threshold Y (POD_Y). Future studies on O_3 impacts on vegetation and related economic losses should move beyond concentration-based metrics and incorporate flux-based approaches (Ronan et al. 2020).

Previous studies in the Czech Republic have reported exceedances of critical levels (*CL*) based on stomatal O_3 flux metrics for both *P. abies* and *F. sylvatica* (Zapletal et al. 2012, 2018; Vlasáková-Matoušková, Hůnová 2015). Therefore, the present study aimed to evaluate the impacts of O_3 on field-based forest stands in the Czech Republic by combining the assessment of visible foliar O_3 injury with both the legislatively established concentration-based AOT40 index and the recommended, biologically meaningful flux-based POD_1 metric. The study is focused on European beech (*Fagus sylvatica* L.) and Norway spruce [*Picea abies* (L.) Karst.], two key tree species of Czech forests. According to National Forest Inventory data, *P. abies* is the dominant tree species, accounting for 45% of the forest area, while the share of *F. sylvatica* in Czech forests is approximately 10% (MoA 2025). Moreover, *F. sylvatica* plays a unique role in forest ecosystems and is considered an ecologically important mixed-forest species, contributing substantially to forest stability, resilience, and biodiversity (Smidt, Herman 2004; Vacek, Balcar 2004; Vacek et al. 2025). The specific objectives were:

(*i*) to assess the phytotoxic potential of O_3 on native tree species using commonly applied O_3 exposure indices (AOT40 and POD_1);

(*ii*) to determine the limitation of stomatal flux due to local environmental conditions;

(*iii*) to examine the relationship between O_3 metrics (AOT40 and POD_1) and the occurrence of visible O_3 foliar injury;

(*iv*) to assess which metric better reflects O_3 phytotoxicity in the Czech Republic.

MATERIAL AND METHODS

Monitoring plots. Eight plots of intensive forest monitoring established within the International Co-operative Programme on Assessment and Monitoring of Air Pollution Effects on Forests (ICP Forests) were selected in different regions of the Czech Republic at altitudes ranging from 350 to 1 300 m above sea level (a.s.l.) (Figure 1, Table 1). These plots are suitable for our study because of the possibility of assessing visible foliar O_3 injury on a light-exposed forest edge at a distance of no more than 500 m from the monitoring plot. There is also a historical connection with older ground-level O_3 studies (Novotný et al. 2010; Boháčová et al. 2011; Šrámek et al. 2012). Attention was paid to the European beech (*F. sylvatica*) and the Norway spruce (*P. abies*).

Meteorological and soil moisture input data. The meteorological and soil moisture data required to calculate POD_1 and to assess the environmental effects on O_3 uptake were obtained from numerical models. Meteorological data [air temperature (*Temp*), relative air humidity (*RAH*), surface solar radiation downward (*SSRD*), atmospheric pressure, and friction velocity] were taken from the ALADIN model (Termonia et al. 2018), which is routinely operated by the Czech Hydrometeorological Institute (CHMI). The variables were available with a spatial resolution of 1 h and a temporal resolution of 2.3 km × 2.3 km.

Soil moisture data were obtained from the ECMWF ERA5-Land meteorological reanalysis (Mu-

https://doi.org/10.17221/24/2026-JFS

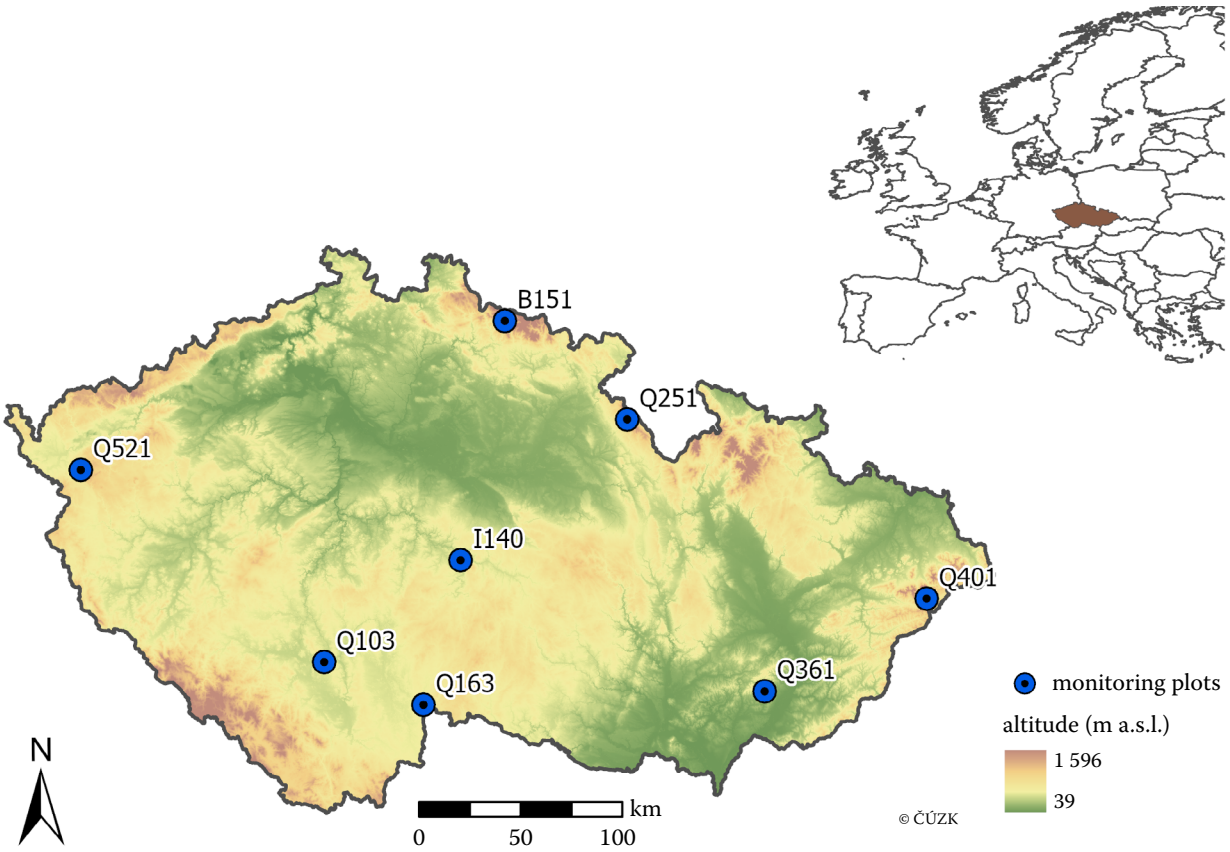

Figure 1. The location of the experimental plots

Table 1. Basic characteristics of the evaluated plots

Plot code	Plot name	Position		Altitude (m a.s.l.)
B151	Mísečky	50°43'48"N	15°33'00"E	940
I140	Želivka	49°40'12"N	15°13'48"E	440
Q103	Všeteč	49°13'12"N	14°18'36"E	615
Q163	Lásenice	49°01'48"N	14°58'48"E	595
Q251	Luisino údolí	50°17'24"N	16°23'24"E	940
Q361	Medlovice	49°04'12"N	17°16'48"E	350
Q401	Klepačka	49°27'00"N	18°23'24"E	650
Q521	Lazy	50°03'00"N	12°37'48"E	875

ñoz-Sabater 2019). The variable volume of water in the soil layer [expressed as m^3 of water per m^3 of ground ($m^3 \cdot m^{-3}$)] was used to represent soil moisture in specific soil layers. For *F. sylvatica*, the volume of water in soil layer 3 (28–100 cm) was applied, whereas for *P. abies*, the volume of water in soil layer 2 (7–28 cm) was used. The choice of soil layers followed the recommendations of the Forestry and Game Management Research Institute (Novotný, personal communication, February 2, 2022) and was further supported by the findings of Kodrík and Kodrík (2002), Schmid (2002), and Oravcová and Vido (2022). The temporal resolution was 1 h and the spatial resolution was 0.1° × 0.1°. The wilting point and field capacity were considered temporally constant and were obtained from the JRC soil database (JRC 2016) with a horizontal resolution of 2 km × 2 km.

https://doi.org/10.17221/24/2026-JFS

O_3 concentrations. Hourly O_3 concentrations at individual plots at a height of 2 m (O_{3_2m}) were extracted from gridded model values. These values were derived by combining measured O_3 concentrations, the chemical transport model, and additional auxiliary data (altitude and the five-year mean gridded O_3 concentrations). These datasets were combined using a linear regression model, followed by kriging of the residuals obtained from this model (for more details, see Horálek et al. 2025). Hourly measured O_3 concentrations were obtained from the Air Quality Information System database, operated by the CHMI, for 27 stations classified as rural background sites (automated monitoring stations that are part of the National Air Quality Monitoring Network operated by the CHMI). For the purpose of spatial interpolation, outputs from the chemical transport model CAMx (2.3 km × 2.3 km resolution; Ramboll US Consulting 2018), in the configuration routinely used for annual air quality assessments by the CHMI, were applied.

The hourly O_3 concentration at the top of the canopy (O_{3_canopy}) was then estimated using the tabulated O_3 vertical gradients recommended by CLRTAP (2024), according to Equation (1):

$$O_{3\_canopy} = O_{3\_2m} \times \frac{g(z_1)}{g(z_m)} \quad (1)$$

where:

O_{3_canopy} – the O_3 concentration at the canopy top (ppb);
O_{3_2m} – the O_3 concentration at the reference height z_m (2 m; ppb);
$g(z_1)$ – the O_3 gradient factor for canopy height (equal to 1 for trees with a height of 20 m);
$g(z_m)$ – the O_3 gradient factor for the measurement height (equal to 0.95 for O_3 concentration measured at 2 m).

Calculation of AOT40F. AOT40F was calculated from hourly O_{3_canopy} concentrations at a particular plot for the vegetation season. Considering the usual leaf unfolding and autumn leaf colouring time of *F. sylvatica*, the onset of current year needles of *P. abies*, and the mean day when the survey of symptoms was carried out, the evaluation period was set from 15 May to 15 September of the respective year. AOT40F (expressed in ppm·h) was calculated as the sum of the difference between hourly concentrations greater than 40 ppb and 40 ppb over a given period using only the 1-h values of O_{3_canopy} concentration during daylight hours (when *SSRD* exceeds 50 W·m^{-2}). The *CL* of AOT40F is set at 5 ppm·h (CLRTAP 2024).

Calculation of POD_Y. POD_Y was calculated following the methodology described in the most recent revision of the Manual on Methodologies and Criteria for Modelling and Mapping Critical Loads and Levels and Air Pollution Effects, Risks, and Trends (CLRTAP 2024; originally CLRTAP 2017). The formulation of the stomatal flux model and *POD* calculation remains unchanged compared to the previous version, while the 2024 update primarily reflects editorial consolidation. The time span was the same as for AOT40F, that is, from 15 May to 15 September of the respective year.

The basis for the POD_Y calculation is the estimation of the instantaneous stomatal conductance (g_{sto}) for each hour H, defined as shown by Equation (2):

$$g_{sto} = g_{max} \times f_{phen} \times f_{light} \times \times \max[f_{min}, (f_{temp} \times f_{VPD} \times f_{SW})] \quad (2)$$

where:

g_{sto} – actual stomatal O_3 conductance (mmol O_3·m^{-2} PLA·s^{-1});
g_{max} – species-specific maximum stomatal O_3 conductance (mmol O_3·m^{-2} PLA·s^{-1});
f_{phen} – phenological development stage;
f_{min} – minimum relative stomatal conductance during daylight.

The functions f_{temp}, f_{VPD}, f_{SW}, and f_{light} represent the relative effects of temperature, vapour pressure deficit, soil water content, and *SSRD* on stomatal behaviour. These *f*-values are expressed as relative functions (values between 0 and 1) representing the fraction of g_{max} under specific environmental conditions. Their functional forms were applied following the algorithms reported in Chapter 3 of the mapping manual (CLRTAP 2024). All parameters required to calculate POD_Y were adopted from the methodology and its species-specific parameterisation (Table 2) presented in CLRTAP (2024).

The only modification concerned the calculation of f_{SW}, which was replaced by f_{SMI} (the soil moisture index), taking values between 0 and 1 as a proportion of g_{max} (with 0 for soil moisture at or below the wilting point). The basic Equation (3) used for f_{SW} resp. f_{SMI} is:

https://doi.org/10.17221/24/2026-JFS

Table 2. Summary of the parameters in the stomatal conductance model for *Fagus sylvatica* and *Picea abies* (CLRTAP 2024)

Tree species	g_{max} (mmol O_3·m^{-2} PLA·s^{-1})	f_{min} (fraction)	$light_a$	T_{min} (°C)	T_{opt} (°C)	T_{max} (°C)	VPD_{max} (kPa)	VPD_{min} (kPa)
Fagus sylvatica	155	0.13	0.006	5	16	33	1.0	3.1
Picea abies	130	0.16	0.010	0	14	35	0.5	3.0

g_{max} – maximum stomatal O_3 conductance; f_{min} – minimum stomatal conductance; $light_a$ – determines the relationship of stomatal response to light; T_{max}, T_{opt}, and T_{min} – maximum, optimum, and minimum temperature, respectively; VPD_{min} and VPD_{max} – *VPD* where g_{sto} is at its minimum and maximum, respectively

$$\begin{aligned} f_{SMI} &= 0 && \text{for } SMI \le 0 \\ f_{SMI} &= SMI/SMI_t && \text{for } 0 < SMI \le SMI_t \\ f_{SMI} &= 1 && \text{for } SMI > SMI_t \end{aligned} \quad (3)$$

$$\text{when} \quad SMI = \frac{SWLL - PWP}{FC - PWP}$$

where:

SMI_t – threshold *SMI*, set to 0.5, above which stomatal conductance is at a maximum;

SWLL – soil moisture (m^3·m^{-3});

PWP – permanent wilting point (m^3·m^{-3});

FC – field capacity (m^3·m^{-3}).

The EMEP methodology (Simpson et al. 2012; CLRTAP 2020) was used to determine f_{SMI}. The *SMI* has an advantage over volumetric methods because it is less sensitive to local soil characteristics; thus, it is easier to interpolate across different vegetation types and grids (Simpson et al. 2012). Using f_{SMI} offers a more practical and robust alternative for representing soil moisture stress in large-scale modelling (CLRTAP 2020). This approach to calculate f_{SMI} is also called the plant available water (PAW) approach, as highlighted by Büker et al. (2012).

Then, the hourly stomatal O_3 flux was calculated according to Equation (4):

$$F_{sto} = O_{3\_canopy} \times g_{sto} \times \frac{r_c}{r_b + r_c} \quad (4)$$

where:

O_{3_canopy} – the O_3 concentration at the canopy top (after unit conversion: nmol·m^{-3});

g_{sto} – actual stomatal O_3 conductance (after unit conversion: m·s^{-1});

r_b – quasi-laminar resistance (s·m^{-1});

r_c – leaf surface resistance (s·m^{-1}).

Hourly averaged stomatal O_3 fluxes (F_{sto}) exceeding threshold *Y*, expressed in nmol·m^{-2} PLA·s^{-1}, are summed over a species- or vegetation-specific accumulation period to obtain POD_Y, using Equation (5):

$$POD_Y = \sum_{i=1}^{n} \max\left(F_{sto,i} - Y, 0\right) \times \Delta t \quad (5)$$

where:

Y – the threshold value, subtracted from each hourly F_{sto} (nmol·m^{-2} PLA·s^{-1}) value only when $F_{sto} > Y$, and only during daylight hours defined as periods when *SSRD* exceeds 50 W·m^{-2};

n – number of hours included in the calculation;

Δt = 1 h;

i – the summation index that represents all hourly time steps within the accumulation period that meet these conditions.

For trees, threshold *Y* (representing the threshold below which it is assumed that any O_3 molecule absorbed by the plant will be detoxified; Mills et al. 2011) was set to 1 nmol·m^{-2} PLA·s^{-1}. Thus, POD_1 (mmol·m^{-2} PLA) represents the accumulated stomatal O_3 uptake above this threshold. When the calculated POD_1 exceeds the flux-based *CL*, the difference defines the critical level exceedance ($CL_{exceedance}$), see Equation (6):

$$CL_{exceedance} = POD_1 - \text{critical level} \quad (6)$$

where:

POD_1 – phytotoxic ozone dose above a flux threshold of 1 nmol O_3 m^{-2}·s^{-1} per leaf area.

The *CL* for *F. sylvatica* was set at 5.2 mmol·m^{-2} PLA (potential effect at this *CL* is a 4% annual reduction of the whole tree biomass). The *CL* for *P. abies* was set be to 9.2 mmol·m^{-2} PLA (potential ef-

https://doi.org/10.17221/24/2026-JFS

fect at this *CL* is a 2 % annual reduction of the whole tree biomass). The date of the exceedance of the *CL* was also determined for each plot and vegetation season.

Data processing and harmonisation to calculate O_3 indices. All variables were initially modelled for the entire territory of the Czech Republic. The resulting data were subsequently processed and harmonised on a common computational grid with a spatial resolution of 1 km × 1 km, which served as the input domain to calculate POD_1. For each experimental plot, hourly values of the relevant variables (O_{3_canopy}; POD_1; air temperature; *RAH*; *SSRD*; soil moisture; and the stomatal response functions f_{temp}, f_{VPD}, f_{SMI}, f_{light}, and g_{sto}) were extracted from the 1 × 1 km grid cell corresponding to the plot location and used in further analyses.

Assessment of visible foliar O_3 injury. The method of symptom assessment has been described in detail (see part VIII 'Assessment of O_3 injury', Schaub et al. 2020). The assessment was performed on light-exposed sampling site (LESS) plots. These plots were exposed to full sunshine on an open plot area (i.e. forest edges), preferably with south or south-west exposure. Each LESS plot was divided into non-overlapping quadrats (2 m × 1 m), and quadrats were randomly selected (the number depended on the length of the LESS plot).

Subsequently, the visible foliar O_3 injury of *F. sylvatica* and *P. abies* was assessed on each LESS plot. From the randomly selected quadrats, only those containing *F. sylvatica* or *P. abies* were considered. The number of quadrats with visible foliar O_3 injury on *F. sylvatica* or *P. abies* was recorded. Then, the relative frequency of visible foliar O_3 injury [Equation (7) below] was calculated for each species (Manzini et al. 2023). Visible foliar O_3 injury was assessed on fully developed leaves exposed to full sunlight.

O_3 foliar symptoms were assessed by two well-trained observers who regularly participate in the Field Ozone Intercalibration Course organised by ICP Forests. Several comparative documents were used to confirm the O_3 effect (Innes et al. 2001; Novotný et al. 2009; Carrari et al. 2020) to exclude ambiguous symptoms caused by, for example, fungal disease or heat stress (Novotný et al. 2009; Schaub et al. 2020).

Statistical analysis. Statistical analyses were conducted using the R software environment (R Core Team 2024). The dataset comprised 18 groups of variables (e.g. meteorological, environmental, and physiological parameters, and O_3 indices), each consisting of three time points corresponding to the 2021, 2022, and 2023 vegetation seasons. Due to the small number of observations (n = 8 per group) and the repeated-measures design (same location measured in all three years), data normality was not formally tested, and non-parametric methods were applied. For all analyses, $P < 0.05$ was considered to indicate a statistically significant result.

Differences among years within each variable group were assessed using the Friedman test, which accounts for repeated measures. For groups where the Friedman test indicated statistically significant differences ($P < 0.05$), post hoc pairwise comparisons were performed using the Wilcoxon signed-rank test for paired samples, with Holm's correction applied to adjust for multiple testing. An adjusted P-value < 0.05 was considered to indicate a statistically significant result.

Random forest analysis (RFA) is a non-parametric, tree-based ensemble learning method for regression and classification (Breiman 2001) that allows the ranking of predictor variables according to their relative importance in explaining the response variable (Sicard et al. 2020).

In this study, RFA was applied to assess the relative importance of environmental variables in determining POD_1 for *F. sylvatica* and *P. abies* during the 2021–2023 vegetation seasons. Weekly means of environmental variables were calculated from hourly data during active daytime periods ($SSRD > 50$ W·m^{-2}). The predictor variables included air temperature, soil moisture, *RAH*, *SSRD*, and the O_{3_canopy} concentration, while the response variable was POD_1. To facilitate comparison between sites and years, importance values were normalised within each site to a range between 0 and 1, with the most influential variable assigned a value of 1 (Araminienė et al. 2019; Eghdami et al. 2022).

The dependence of the O_3 concentrations, AOT40F, and POD_1 on altitude, the depend-

$$\text{Symptomatic quadrats on the LESS (\%)} = \frac{\text{number of LESS quadrats with symptoms}}{\text{total number of LESS quadrats with present } \textit{Fagus sylvatica} \text{ or } \textit{Picea abies}} \times 100 \quad (7)$$

https://doi.org/10.17221/24/2026-JFS

ence of visible O_3 injury expressed as a percentage of symptomatic quadrats along LESS plots, and the percentage of symptomatic species at the plot on AOT40F were assessed using nonparametric Spearman rank correlation analysis.

RESULTS

Meteorological and environmental conditions. Meteorological and environmental variables showed distinct interannual patterns across the study period (Table 3). Air temperature increased significantly between all years, while *RAH* declined significantly from 2021 to both 2022 and 2023. In contrast, the difference between 2022 and 2023 was not statistically significant. Soil moisture exhibited site-specific variability, with a general decline across most plots that was particularly pronounced at Q361 and Q521. A statistically significant decrease was observed only between 2021 and 2023 for *F. sylvatica*. *SSRD* showed relatively low interannual variability, with significantly higher values in 2023 compared to 2021, but no significant differences between adjacent years. Overall, the results indicate a shift towards warmer and drier conditions over the study period, with 2021 representing the coolest and most humid season and 2023 the warmest and driest.

Meteorological and environmental conditions for stomatal O_3 conductance. Plot-level evaluation indicated a higher variability of meteorological and environmental conditions for stomatal O_3 conductance in 2022 and 2023 compared with 2021 (Figures 2, 3). While f_{temp} and f_{light} values exhibited a relatively constant range across plots, with the f_{light} values consistently remaining within a narrow range of favourable conditions for stomatal O_3 conductance, f_{SMI} and f_{VPD} showed greater variability. In particular, f_{SMI} values showed a wide range, indicating a limitation of stomatal O_3 conductance at some plots, especially for Q361 and Q521 in 2022 and 2023.

The f_{temp} values (seasonal means across plots) were significantly higher in 2021 than in 2022 only for *P. abies*. The f_{VPD} values for both tree species significantly decreased from 2021 to both 2022 and 2023, with no significant difference between the latter two years. The f_{SMI} and f_{light} values for both tree species did not differ significantly among the vegetation seasons, however, f_{SMI} values were generally highest in 2021. For *F. sylvatica*, the g_{sto}

Table 3. Characteristics of the 2021, 2022, and 2023 vegetation seasons

Plot	*Temp* (°C)			*RAH* (%)			Soil moisture (%), *Fagus sylvatica*			Soil moisture (%), *Picea abies*			*SSRD* ($W \cdot m^{-2}$)		
	2021	2022	2023	2021	2022	2023	2021	2022	2023	2021	2022	2023	2021	2022	2023
B151	12.7 ± 4.7	13.5 ± 5.2	14.2 ± 4.3	80.6 ± 14.7	74.2 ± 16.5	73.9 ± 16.7	37.1 ± 2.4	32.9 ± 3.4	32.7 ± 3.3	37.4 ± 3.2	34.8 ± 4.4	34.0 ± 3.8	208.6 ± 244.5	213.4 ± 253.9	216.8 ± 251.9
I140	16.6 ± 5.1	17.5 ± 5.7	18.4 ± 5.4	74.6 ± 17.7	69.0 ± 21.3	66.2 ± 20.1	34.9 ± 2.3	34.8 ± 3.1	30.4 ± 3.0	35.8 ± 3.2	36.2 ± 3.7	30.5 ± 5.2	213.5 ± 250.0	216.1 ± 259.0	216.6 ± 254.7
Q103	16.7 ± 5.1	17.6 ± 5.5	18.4 ± 5.3	73.1 ± 17.5	69.6 ± 20.4	66.1 ± 19.7	37.0 ± 1.9	35.7 ± 2.6	30.2 ± 3.2	36.8 ± 3.2	36.4 ± 3.5	30.4 ± 4.9	211.1 ± 244.2	214.9 ± 256.6	219.8 ± 257.1
Q163	16.6 ± 5.2	17.4 ± 5.5	18.2 ± 5.2	75.2 ± 17.0	71.6 ± 19.8	69.2 ± 18.6	34.2 ± 1.9	34.3 ± 2.9	30.6 ± 3.2	35.3 ± 3.0	35.5 ± 4.2	30.9 ± 5.6	215.3 ± 249.1	215.1 ± 258.4	220.7 ± 258.5
Q251	14.7 ± 4.7	15.3 ± 5.2	16.0 ± 4.4	77.8 ± 16.3	73.0 ± 17.8	72.7 ± 16.8	33.6 ± 2.3	30.8 ± 3.0	31.6 ± 3.2	35.0 ± 3.5	33.3 ± 4.8	31.6 ± 4.9	208.4 ± 242.9	211.9 ± 251.4	213.6 ± 249.8
Q361	17.5 ± 5.1	18.0 ± 5.4	18.6 ± 4.6	71.0 ± 16.0	68.2 ± 19.8	69.6 ± 16.7	30.8 ± 3.2	23.4 ± 2.5	28.9 ± 3.5	30.7 ± 5.7	25.4 ± 5.5	28.3 ± 6.5	225.2 ± 260.7	219.0 ± 262.9	218.7 ± 258.7
Q401	14.4 ± 5.2	14.8 ± 5.3	15.7 ± 4.5	78.8 ± 15.6	76.5 ± 18.1	75.6 ± 16.9	35.2 ± 4.1	32.9 ± 3.3	34.2 ± 3.6	35.3 ± 4.4	35.0 ± 4.4	35.6 ± 3.5	200.7 ± 238.2	198.8 ± 245.9	202.4 ± 245.1
Q521	14.3 ± 4.6	15.8 ± 5.4	16.3 ± 4.7	80.6 ± 15.7	69.7 ± 19.9	70.6 ± 18.9	36.7 ± 1.4	26.8 ± 3.4	27.6 ± 3.0	36.8 ± 2.8	28.1 ± 6.0	27.8 ± 5.4	201.3 ± 237.1	212.8 ± 250.6	220.4 ± 253.5
All	15.4 ± 5.2	16.2 ± 5.6	17.0 ± 5.1	76.5 ± 16.7	71.5 ± 19.4	70.5 ± 18.4	34.9 ± 3.2	31.5 ± 5.1	30.8 ± 3.8	35.4 ± 4.2	33.1 ± 6.0	31.1 ± 5.6	210.5 ± 246.0	212.8 ± 254.9	216.1 ± 253.7

Temp – air temperature; *RAH* – relative air humidity; *SSRD* – surface solar radiation downward; the data are presented as the mean ± standard deviation

https://doi.org/10.17221/24/2026-JFS

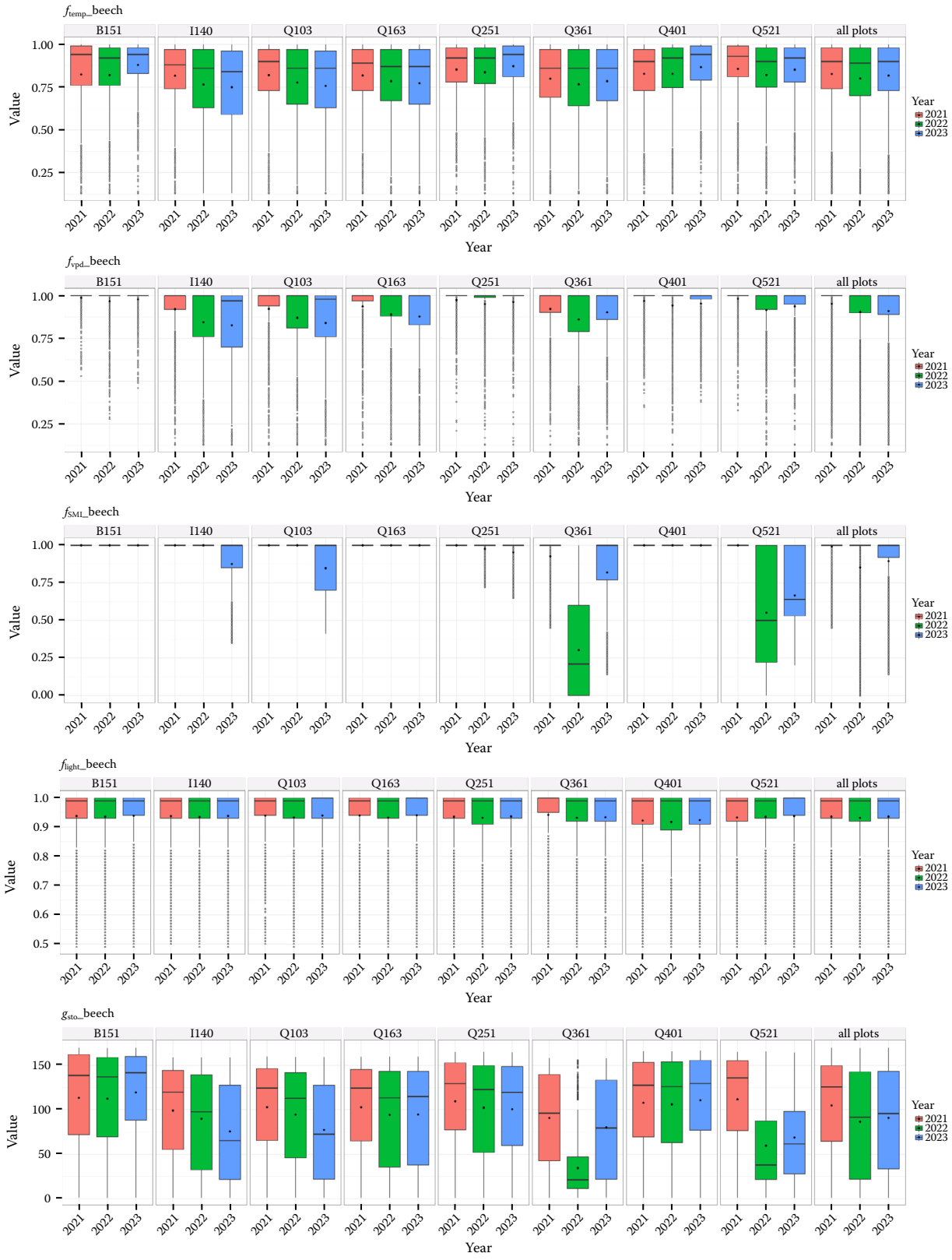

Figure 2. Box plots of environmental factors – the relative effects of temperature (f_{temp}), vapour pressure deficit (f_{VPD}), soil moisture (f_{SMI}), and surface solar radiation downward (f_{light}) – and the actual stomatal O_3 conductance (g_{sto}, mmol·m^{-2} PLA·s^{-1}) for *Fagus sylvatica* in the 2021, 2022, and 2023 vegetation seasons

Black dots – indication of the means

https://doi.org/10.17221/24/2026-JFS

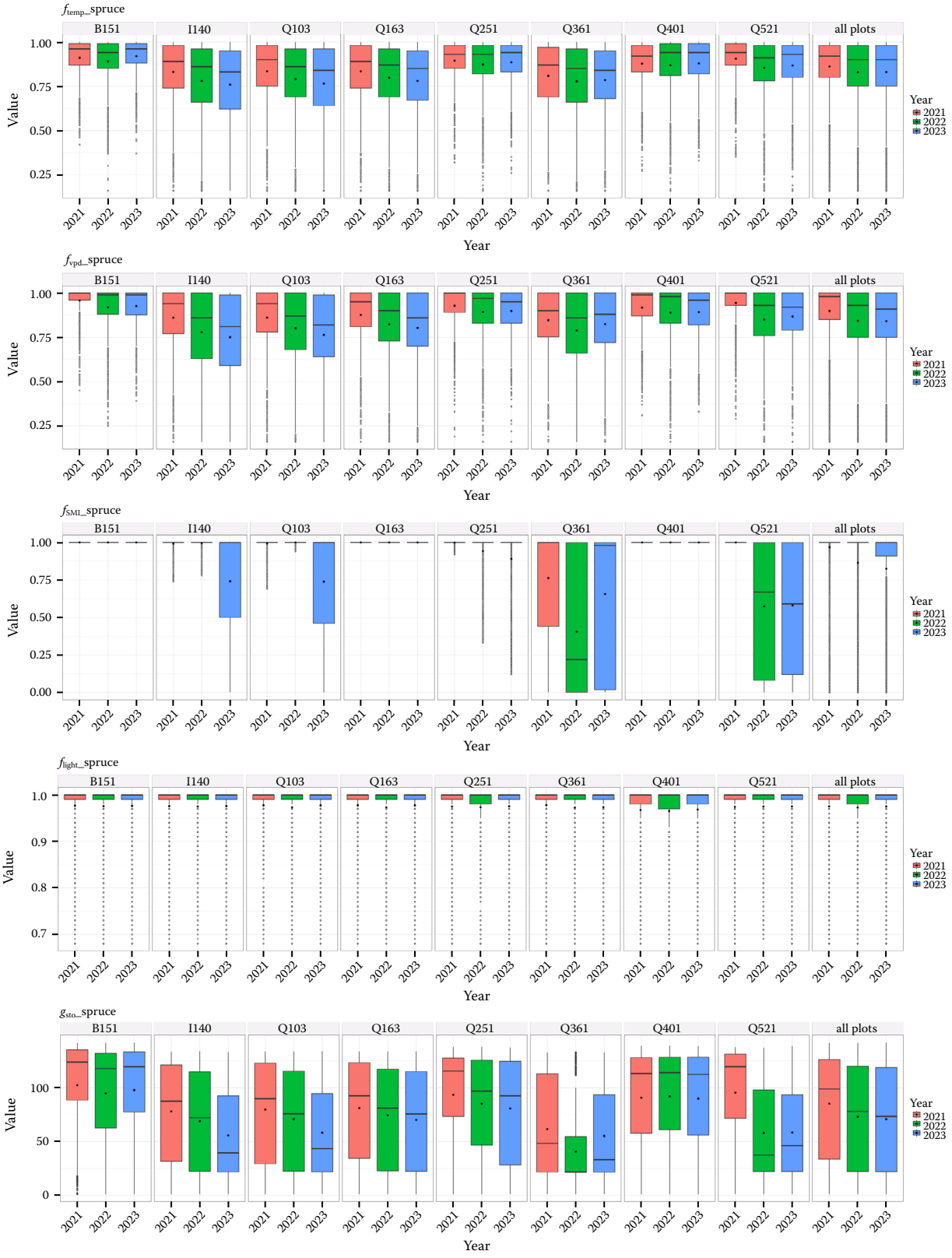

Figure 3. Box plots of environmental factors – the relative effects of temperature (f_{temp}), vapour pressure deficit (f_{VPD}), soil moisture (f_{SMI}), and surface solar radiation downward (f_{light}) – and the actual stomatal O_3 conductance (mmol·m^{-2} PLA·s^{-1}) for *Picea abies* in the 2021, 2022, and 2023 vegetation seasons

Black dots – indication of the means

https://doi.org/10.17221/24/2026-JFS

values differed significantly among all three vegetation seasons, with the highest values in 2021. A similar pattern was observed for *P. abies*, where g_{sto} showed a significant decline from 2021 to 2023. In summary, the most favourable conditions for stomatal O_3 conductance for both species were observed in 2021, which was reflected in higher g_{sto} values.

RFA. Based on RFA, air temperature, soil moisture, and O_{3_canopy} were identified as the main factors influencing stomatal O_3 flux during the period of 2021–2023. The relevance of soil moisture in determining stomatal conductance increased particularly in 2022 and 2023, especially for plots characterised by the highest variability in the soil water availability (I140, Q103, Q251, Q361, and Q521; Figures 2 and 3). In contrast, *RAH* and *SSRD* showed consistently low relative importance across all sites and years (Table 4).

O_3 concentrations. Seasonal mean O_3 concentrations increased gradually over the three-year period (Table 5). There was significant interan-

Table 4. Results of random forest analysis – relative importance of environmental variables [air temperature (*Temp*), relative air humidity (*RAH*), soil moisture, surface solar radiation downward (*SSRD*), and O_{3_canopy} concentrations] for POD_1, averaged for the 2021–2023 vegetation seasons

Plot	B151	I140	Q103	Q163	Q251	Q361	Q401	Q521
Fagus sylvatica								
Temp (°C)	0.5	**0.9**	**0.8**	**0.9**	0.7	**0.6**	0.7	**0.5**
SSRD ($W \cdot m^{-2}$)	**0.7**	0.3	0.3	0.0	**0.9**	0.3	**0.8**	0.3
RAH (%)	0.2	0.4	0.3	0.3	0.4	0.2	0.3	0.2
Soil moisture (%)	0.2	**0.8**	**0.7**	**0.9**	0.3	**1.0**	0.2	**0.7**
O_3 concentration (ppb)	**0.6**	0.2	0.2	0.3	**0.9**	0.3	**0.9**	**0.5**
Picea abies								
Temp (°C)	**0.9**	**1.0**	**1.0**	**1.0**	**0.9**	**0.5**	**0.7**	**0.5**
SSRD ($W \cdot m^{-2}$)	**0.8**	0.2	0.4	0.2	0.3	0.3	0.3	0.1
RAH (%)	0.5	**0.6**	0.4	0.3	0.1	0.3	0.0	0.4
Soil moisture (%)	0.2	0.3	0.4	**0.5**	**0.8**	**1.0**	**0.6**	**0.8**
O_3 concentration (ppb)	**0.8**	0.1	0.2	0.3	0.2	0.3	0.5	0.5

Bold – the main factors influencing stomatal O_3 flux during the period of 2021–2023

Table 5. Seasonal O_3 concentrations (mean ± standard deviation) and AOT40F and POD_1 values for the 2021, 2022, and 2023 vegetation season for *Fagus sylvatica* and *Picea abies*

Plot	O_3 (ppb)			AOT40F (ppm·h)			POD_1 for beech ($mmol \cdot m^{-2}$ PLA)			POD_1 for spruce ($mmol \cdot m^{-2}$ PLA)		
	2021	2022	2023	2021	2022	2023	2021	2022	2023	2021	2022	2023
B151	39.0 ± 10.1	42.6 ± 11.6	44.1 ± 10.1	10.7	16.0	17.0	18.0	19.9	21.8	20.9	21.5	23.3
I140	34.5 ± 11.0	36.4 ± 12.5	39.1 ± 11.2	9.3	13.5	15.4	15.6	14.4	12.8	15.0	13.4	10.3
Q103	35.0 ± 10.1	37.1 ± 11.4	39.5 ± 10.6	8.3	12.3	14.9	15.9	15.3	13.3	15.3	14.2	11.0
Q163	35.0 ± 10.3	36.3 ± 11.7	39.0 ± 10.4	8.4	11.6	13.7	16.6	15.8	16.6	15.8	14.7	15.0
Q251	40.1 ± 10.0	43.3 ± 11.6	44.1 ± 10.2	11.4	15.9	16.7	18.1	18.2	19.1	19.7	18.3	18.1
Q361	36.4 ± 11.1	37.9 ± 12.4	38.4 ± 10.9	11.3	14.4	13.4	14.7	4.7	12.9	11.7	5.5	9.9
Q401	38.3 ± 10.4	37.9 ± 11.6	41.1 ± 10.3	11.2	11.7	13.7	19.3	18.0	20.5	19.3	17.6	19.5
Q521	36.6 ± 10.4	41.0 ± 11.2	41.9 ± 10.5	8.8	15.2	16.3	17.7	9.1	13.4	19.1	10.6	10.8
All	36.9 ± 10.6	39.1.0 ± 12	40.9 ± 10.7	9.9	13.8	15.1	17.0	14.4	16.3	17.1	14.5	14.7

O_3 – ground-level ozone; AOT40F – accumulated O_3 concentration above 40 ppb for forest protection; POD_1 –phytotoxic ozone dose above a flux threshold of 1 nmol O_3 $m^{-2} \cdot s^{-1}$ per leaf area

https://doi.org/10.17221/24/2026-JFS

nual variability in O_3 concentrations. Plots located at higher altitudes (B151, Q251, and Q521) consistently exhibited the highest O_3 concentrations. There was a significant correlation between O_3 concentrations and altitude for all three vegetation seasons (Figure 4).

In terms of seasonal dynamics, monthly mean O_3 concentrations ranged from 30.0 ppb to 47.9 ppb in 2021, from 26.7 ppb to 47.9 ppb in 2022, and from 35.3 ppb to 48.8 ppb in 2023. Monthly mean concentrations varied considerably throughout each vegetation season. In all three years, O_3 concentrations peaked in June and July, with a maximum monthly mean of 47.9 ppb in 2021 and 2022, and 48.8 ppb in 2023. The lowest monthly means were recorded in August or September, depending on the year.

AOT40F. At all sites, the *CL* of AOT40F was exceeded in every vegetation season (Figure 5). Similarly to the O_3 concentrations, AOT40 increased gradually over the three-year period (Table 5). There was significant interannual variability in AOT40F. Moreover, there was a significant correlation between AOT40F and altitude for the 2023 vegetation season (Figure 4).

The average day of *CL* exceedance shifted earlier each year: July 5 in 2021 (day 186), June 27 in 2022 (day 178), and June 24 in 2023 (day 175). The magnitude of *CL* exceedance ranged from 66% to 240% at individual plots during the 2021–2023 period. Both shifts corresponded with the trend for increasing O_3 concentrations observed during the 2021–2023 period.

***POD*$_1$.** At all sites, the *CL* of POD_1 for *F. sylvatica* and for *P. abies* was exceeded every vegetation season, except at Q361 in 2022 (Table 5 and Figure 5). For *F. sylvatica*, four plots reached their maximum POD_1 in 2021, and the other four in 2022. For *P. abies*, six plots reached their maximum POD_1 in 2021 and two plots in 2023. POD_1 values showed no significant interannual variation, with a slight decrease in 2022 and partial recovery in 2023 for *F. sylvatica*, and minor, irregular changes for *P. abies*, indicating a stronger influence of environmental conditions than interannual variation in O_3 concentrations (Table 5). POD_1 and altitude

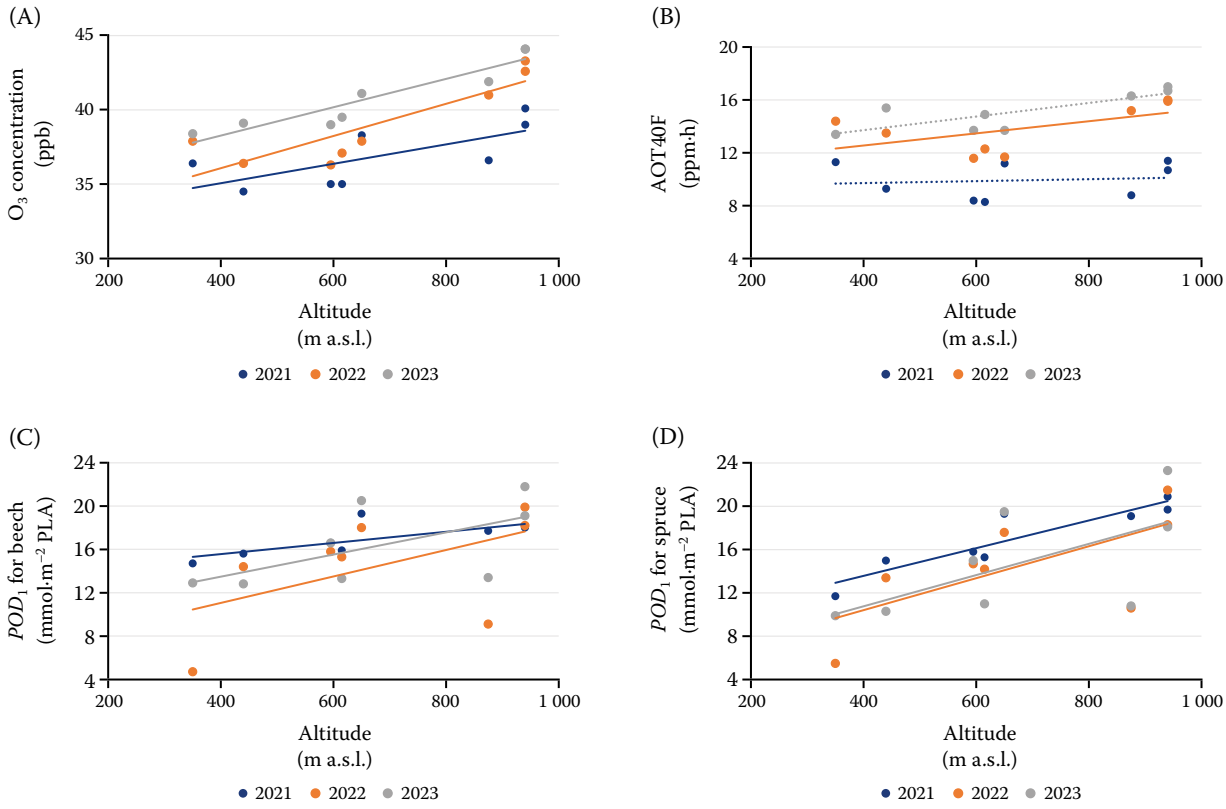

Figure 4. Relationships between the (A) O_3 concentration, (B) AOT40F, and (C) POD_1 for *Fagus sylvatica*, and (D) POD_1 for *Picea abies* and altitude

Solid lines – statistically significant correlations

https://doi.org/10.17221/24/2026-JFS

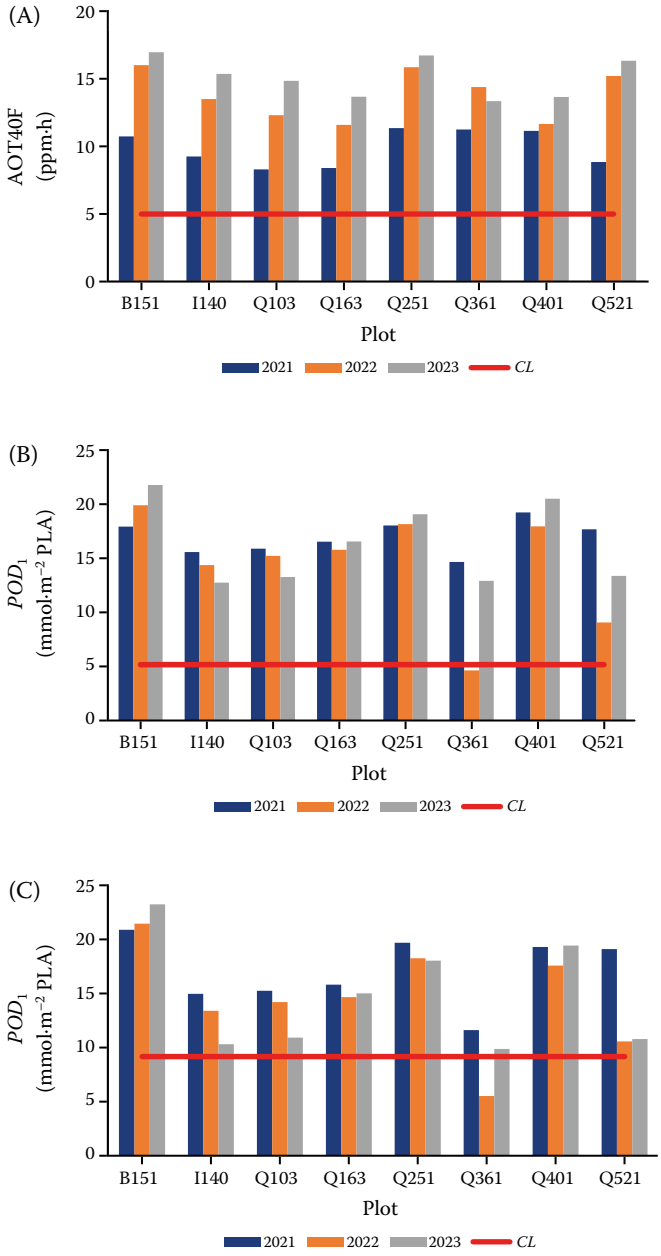

Figure 5. AOT40F and POD_1 at individual plots during the 2021–2023 growing seasons: (A) AOT40F, (B) POD_1 for *Fagus sylvatica*, and (C) POD_1 for *Picea abies*

Red line – critical level (*CL*)

showed a significant correlation for all three vegetation seasons (Figure 4).

For *F. sylvatica*, the POD_1 threshold was typically exceeded first, followed by AOT40. In contrast, for *P. abies*, POD_1 exceedance was observed after AOT40, later in the season (Figure 6). The average day of *CL* exceedance for *F. sylvatica* remained relatively consistent across the three vegetation seasons, occurring around mid-June. For *P. abies*, the average day of *CL* exceedance was July 25 in 2021, July 30 in 2022, and August 11 in 2023, showing a tendency towards later exceedance in recent years. The magnitude of *CL* exceedance varied among the plots and years, ranging from 75% to 319% for *F. sylvatica* and from 8% to 153% for *P. abies* at individual plots during the 2021–2023 period, suggesting a high risk of O_3-induced damage to forest vegetation.

Visible foliar O_3 injury. *F. sylvatica* showed limited visible foliar O_3 injury, observed at four plots in 2022 and at three plots in 2023 (Table 6).

https://doi.org/10.17221/24/2026-JFS

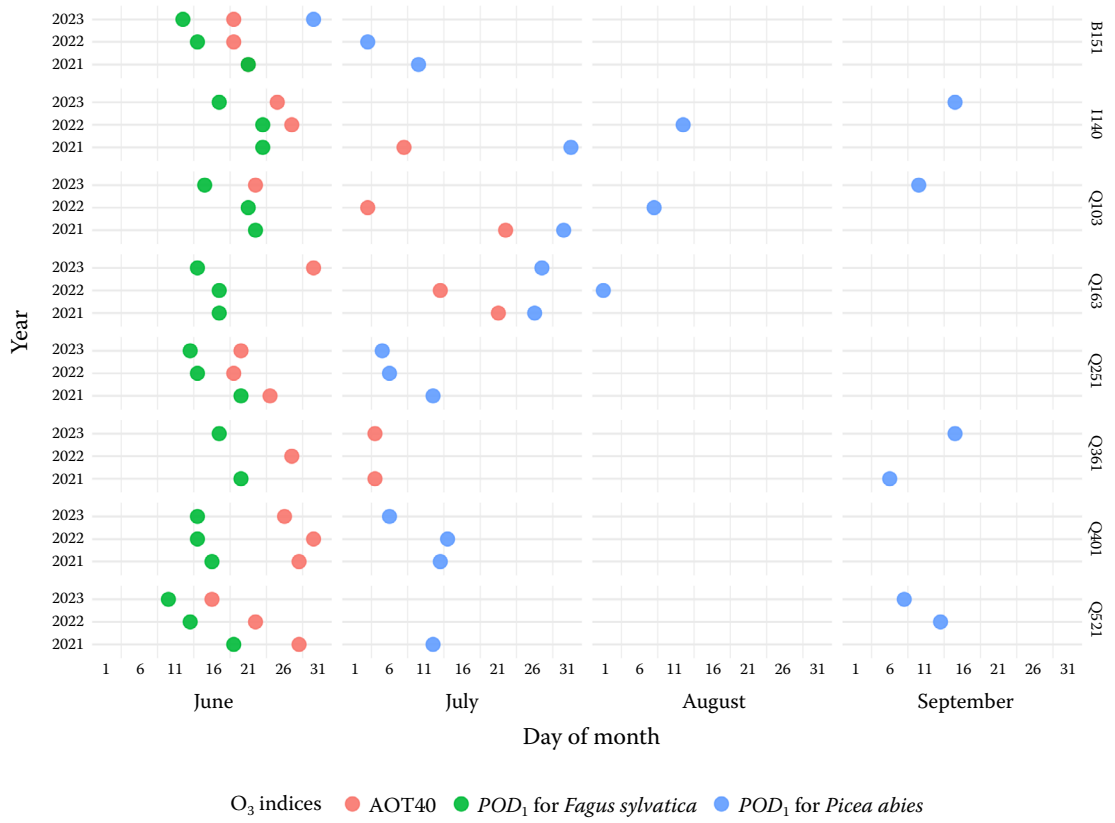

Figure 6. Exceedance days of O_3 critical levels for *Fagus sylvatica* and *Picea abies* across the plots and years

For *P. abies*, when assessing the needles from the current year, there was no visible foliar O_3 injury for any of the observation years (2021–2023). The response of visible foliar O_3 injury, expressed as the percentage of symptomatic quadrats (i.e. visible foliar O_3 injury observed on *F. sylvatica* leaves), to O_3 metrics (AOT40 and POD_1) was analysed for individual vegetation seasons 2021–2023 and for the means across all sites and years (Figure 7). There were no statistically significant correlations between the O_3 metrics and the occurrence of visible foliar injury on *F. sylvatica*. However, the graphical pattern suggests a slightly stronger positive association between visible foliar O_3 injury and POD_1 compared with AOT40, for which there was no clear relationship (Figure 7).

Table 6. Symptomatic quadrats on the light-exposed sampling site (LESS) plots in 2021, 2022 and 2023 – *Fagus sylvatica*

Plot	Forest edge with LESS (m)	Number of 2 × 1 m quadrats (adjusted sample size)		2-m non-overlapping quadrats with symptomatic *Fagus sylvatica* (%)		
		in total	with *Fagus sylvatica*	2021	2022	2023
B151	140	33	3	0	0	0
I140	40	17	17	0	12	18
Q103	120	33	12	0	0	0
Q163	165	33	33	0	9	9
Q251	165	33	10	0	30	50
Q361	60	23	6	0	0	0
Q401	50	20	10	0	20	30
Q521	100	33	8	0	0	0

https://doi.org/10.17221/24/2026-JFS

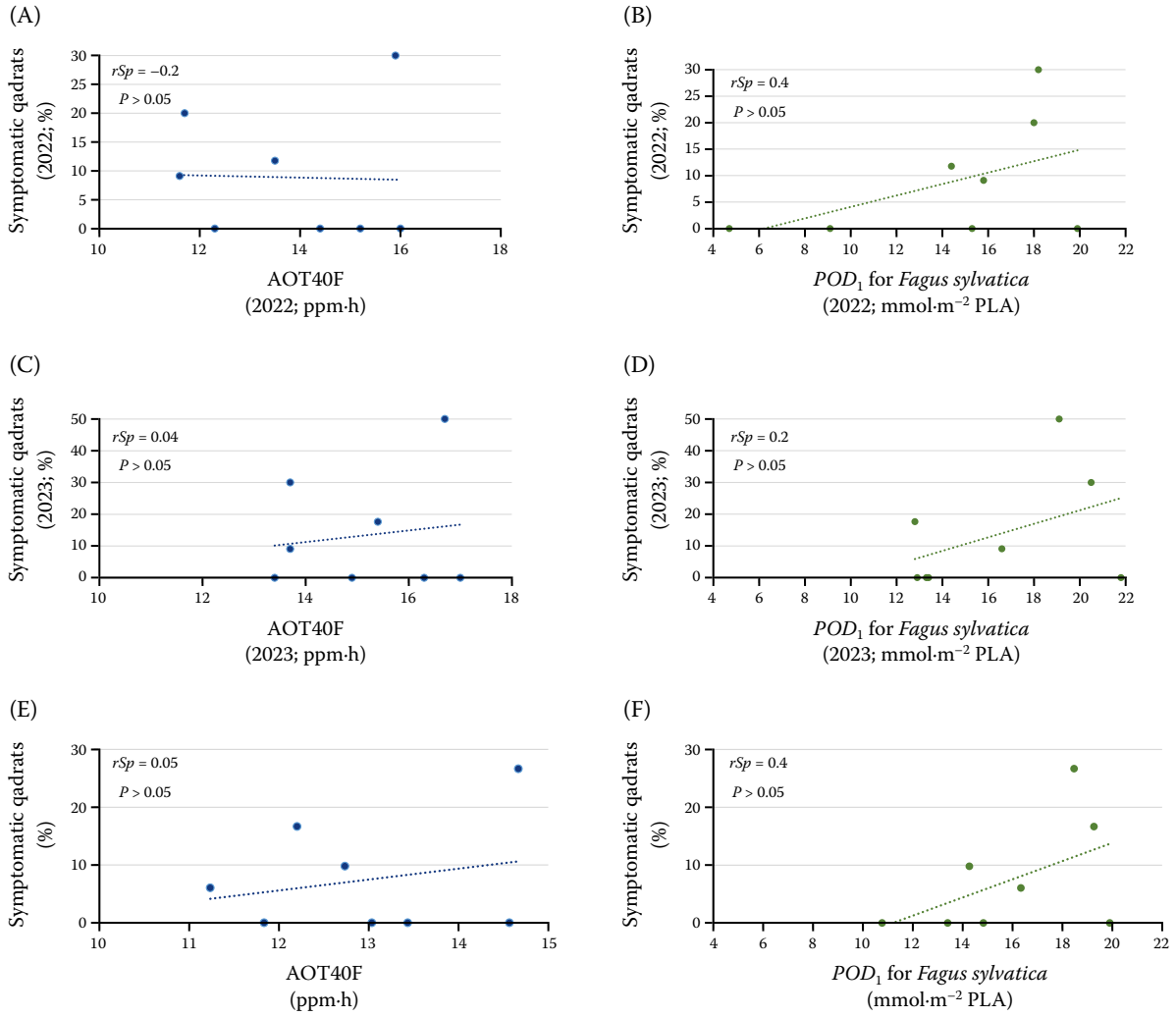

Figure 7. Relationships between mean O_3 indices and visible foliar injury in *Fagus sylvatica*: (A, C, E) AOT40 and (B, D, F) POD_1
Panels represent the 2022 (A, B) and 2023 (C, D) symptomatic vegetation seasons and the multi-year average for 2021–2023 (E, F); visible injury is expressed as average percentage of symptomatic quadrats

DISCUSSION

O_3 concentrations and O_3 metrics in a Central European context. The seasonal mean O_3 concentrations observed across our sites (36.9 ppb, 39.1 ppb, and 40.9 ppb) fall well within the range reported in previous Central European studies. For example, similar values (41.1 ppb, 36.0 ppb, and 36.8 ppb for the 2006, 2007, and 2008 vegetation seasons, respectively) were reported from the Jizerské hory Mts. (Hůnová et al. 2011; Vlasáková-Matoušková, Hůnová 2015), consistent with the interannual variability observed at our plots. Bičárová et al. (2016) reported a broader range (30.9 ppb to 44.1 ppb) during the 2014 vegetation season at higher–elevation sites (810–1 778 m a.s.l.) compared to our highest plot.

Similarly, the AOT40F values from the present study (9.9 ppm·h, 13.8 ppm·h, and 15.1 ppm·h) fall within the range reported for European forest environments. Bičárová et al. (2016) documented an altitudinal gradient in the High Tatra Mts. from 6.2 ppm·h at 810 m a.s.l. to 10.7 ppm·h at 1 778 m a.s.l., while lower values (9.3 ppm·h) were reported from Lithuanian forests, representing a cooler climate (Araminienė et al. 2019). Across Europe, AOT40 shows substantial spatial variability, ranging from < 7 ppm·h to 24 ppm·h (Paoletti et al. 2019).

For *F. sylvatica*, the mean POD_1 across the plots was 17.0 mmol·m^{-2} PLA, 14.4 mmol·m^{-2} PLA, and 16.3 mmol·m^{-2} PLA. These values fall within ranges reported for temperate European forests, including 12.6–28.8 mmol·m^{-2} PLA at lower-el-

https://doi.org/10.17221/24/2026-JFS

evation German sites (390–690 m a.s.l.; Eghdami et al. 2022). For *P. abies*, the mean POD_1 values (17.1 mmol·m^{-2} PLA, 14.5 mmol·m^{-2} PLA, and 14.7 mmol·m^{-2} PLA) also fall within published ranges. Comparable values were reported in the High Tatra Mts. (13.6–16.2 mmol·m^{-2} PLA; Bičárová et al. 2016), for Bílý Kříž in the Czech Republic (15.6 mmol·m^{-2} PLA at 908 m a.s.l.; Zapletal et al. 2018), and for western Germany (12.7–29.7 mmol·m^{-2} PLA; Eghdami et al. 2022). Overall, the POD_1 values indicate that stomatal O_3 uptake in the observed plots reflects typical regional conditions for both broadleaved and coniferous forest stands.

Temporal and spatial variability of O_3 metrics. The seasonal mean O_3 concentrations increased significantly over the study period, consistent with rising air temperature promoting photochemical O_3 formation (Seinfeld, Pandis 2006; Coates et al. 2016), and AOT40F showed a similar increase. In contrast, POD_1 did not exhibit significant interannual trends for either species, highlighting that flux-based metrics respond primarily to environmental controls on stomatal conductance rather than to O_3 concentrations alone. This pattern is consistent with long-term studies, when divergent trends between AOT40 and POD_1 have been observed. For example, De Marco et al. (2019) found a decrease in O_3 concentrations and AOT40, while POD_1 showed no significant trend. Similarly, Araminienė et al. (2019) reported a decline in O_3 and AOT40, while POD_1 increased due to enhanced stomatal O_3 uptake under favourable climatic conditions.

This divergence is further reflected in the timing of critical level (*CL*) exceedances. At all plots, the *CL*s for both AOT40F and POD_1 were exceeded in every vegetation season except for Q361 in 2022. For AOT40F, there was a gradual shift towards earlier exceedance dates, indicating increasing O_3 exposure from the 2021 to the 2023 vegetation season. This pattern is consistent with the findings of Bičárová et al. (2016), who also reported the earliest exceedance of concentration-based *CL* occurring in June.

For *F. sylvatica*, the POD_1 *CL* was exceeded in mid-June, compared to mid-May to early June reported by Eghdami et al. (2022). Together, these results indicate that the POD_1 *CL* is exceeded within a relatively narrow time window. For *P. abies*, exceedance of the POD_1 *CL* occurred later, predominantly in July and August, sometimes extending into September; this is partly consistent with early July exceedance observed by Bičárová et al. (2016). In contrast, Eghdami et al. (2022) reported POD_1 *CL* exceedance for *P. abies* between mid-May and late June. The different timing of *CL* exceedance for AOT40F and POD_1 confirms that flux-based metrics respond more sensitively to actual environmental conditions than concentration-based metrics, whereas AOT40F essentially reflects the temporal pattern of O_3 concentrations. Consequently, high POD_1 values can occur even where O_3 concentrations are moderate, but an optimal combination of mild temperatures and no water stress is present (Anav et al. 2022). This is also evident at our plots, where the highest POD_1 values were observed at plots B151 and Q401, which experienced the most favourable conditions for stomatal conductance.

A similar divergence was evident in the spatial (altitudinal) patterns. Both O_3 concentrations and POD_1 increased with altitude, reflecting higher O_3 levels and conditions favouring stomatal openness (Wieser et al. 2000; Díaz-de-Quijano et al. 2009; Brodin et al. 2010; Burley, Bytnerowicz 2011; Dalstein, Ciriani 2019; Bičárová et al. 2019; Eghdami et al. 2022). In contrast, AOT40F showed a significant altitudinal increase only in the year with the highest O_3 concentrations, supporting critiques that AOT40 is not a suitable metric for vegetation risk assessment, as even O_3 concentrations below 40 ppb can be harmful to plants (Matyssek et al. 2004; Nunn et al. 2005).

Relationships between POD_1 and environmental variables. RFA revealed that air temperature, soil moisture, and the O_3 concentration were the dominant regulators of stomatal O_3 uptake at our plots. This finding is in agreement with previous research demonstrating that soil moisture and temperature are key environmental controls on stomatal conductance and on O_3 fluxes. For example, Anav et al. (2016, 2022) showed that the soil water availability is the most important limiting factor for stomatal O_3 fluxes across Europe. Similar patterns were reported by Araminienė et al. (2019) and Sicard et al. (2020) who identified these variables as major predictors of visible O_3 injury and crown condition. Further, soil water stress reduces stomatal conductance and O_3 uptake, while stomatal sluggishness under drought may sometimes intensify O_3 effects (Eghdami et al. 2022).

https://doi.org/10.17221/24/2026-JFS

Visible foliar O_3 injury in *Fagus sylvatica.* In 2022 and 2023, *F. sylvatica* exhibited visible foliar O_3 injury at four plots (I140, Q163, Q251, and Q401), with symptomatic quadrats ranging from 9% to 50%. For broadleaved species, Sicard et al. (2020) proposed a flux-based threshold of 12 mmol·m^{-2} POD_1 for the onset of visible O_3 injury (CL_{vis}). In the present study, symptoms in *F. sylvatica* appeared at 12.8–20.5 mmol·m^{-2}, although no injury was detected in 2021 despite CL_{vis} exceedance at all plots. Similarly, some plots in 2022–2023 exceeded CL_{vis} without developing symptoms. This pattern aligns with reports from other European regions. Sicard et al. (2020) documented both sites with negligible or absent symptoms at relatively high POD_1 (up to 19.5 mmol·m^{-2}) and sites with clear and biologically significant injury. This variability parallels our findings: visible foliar O_3 injury in *F. sylvatica* emerged at some sites and years but not others, even under comparable levels of O_3 exposure.

The results from the present study correspond to those reported for cooler or temperate regions. Araminienė et al. (2019) reported low visible foliar O_3 injury (0–1%) in Lithuanian forests at an average POD_1 of approximately 8 mmol·m^{-2}. In the Jizerské hory Mts. (Czech Republic), Vlasáková-Matoušková and Hůnová (2015) found visible foliar O_3 injury at five of six plots, with symptomatic quadrats ranging from 11% to 56%, closely reflecting the ranges observed in our study. Similarly, Koltay (2025) noted that *F. sylvatica* and other sensitive species exhibited O_3 symptoms, the overall O_3 damage in Hungary remains low. A higher frequency of injuries has been reported in southern or high-altitude areas, where damage can be substantial, with symptomatic quadrats approached 100% (Manzini et al. 2023).

Visible foliar O_3 injury in *F. sylvatica* appeared mainly at plots with the highest POD_1 values (Q163, Q251, and Q401), whereas this pattern was not reflected in AOT40F, with some symptomatic plots (e.g., I140, Q163, and Q401) reaching the lowest AOT40F values. This supports earlier findings showing that visible O_3 injury correlates more strongly with flux-based than concentration-based metrics (Sicard et al. 2016a; Araminienė et al. 2019; Hoshika et al. 2020; Manzini et al. 2023; Viviano et al. 2025).

In the present study, however, there was no significant correlation between POD_1 and visible foliar O_3 injury, either for individual vegetation seasons or when averaged across all three seasons. No relationship was observed even when applying the approach used by Sicard et al. (2016a) – that is, correlating AOT40 or *POD* with visible O_3 injury after joining all data from all sites and years (data not shown). Nevertheless, the graphical patterns indicate a slightly stronger positive association between visible injury and POD_1 than with AOT40F. Thus, although the results from this study do not reproduce the significant flux–injury relationships reported in previous studies, which consistently found stronger flux–injury associations and weak or absent relationships for AOT40 (Hoshika et al. 2020; Sicard et al. 2021; Manzini et al. 2023; Marra et al. 2025; Viviano et al. 2025), they still provide an indication that *POD* may better reflect injury risk than AOT40. This discrepancy is likely due to the limited dataset (n = 24) and the high proportion of zero-injury observations (n = 16), which reduced the statistical power.

Visible foliar O_3 injury in *Picea abies.* Across all plots, *P. abies* exhibited no visible foliar O_3 injury on current-year needles, even though POD_1 exceeded a flux-based *CL* for the onset of visible O_3 injury (CL_{vis}) of 5 mmol·m^{-2} for conifer species (Sicard et al. 2016a). This pattern is consistent with earlier studies describing *P. abies* as an O_3-tolerant species (Nunn et al. 2002; Sicard et al. 2016a) and with regional findings in which conifers exhibited visible foliar O_3 injury only very rarely across several years of observation (Manzini et al. 2023). Therefore, the lack of symptoms likely reflects strong physiological protection rather than the absence of phytotoxic exposure. One contributing mechanism may be drought-induced stomatal regulation. As an isohydric 'drought avoider', *P. abies* rapidly closes its stomata under declining soil moisture or elevated VPD, thereby reducing O_3 flux (Agyei 2020). This is consistent with the findings from plots Q521 and Q361, where the least favourable soil-moisture conditions during 2022–2023 coincided with the lowest POD_1 values in the dataset.

CONCLUSION

This study presents a three-year (2021–2023) assessment of O_3 exposure and stomatal O_3 flux in forest stands across eight monitoring plots in the Czech Republic. The analysis was based on a combination of modelled and measured data, including gridded O_3 concentrations derived from

https://doi.org/10.17221/24/2026-JFS

chemical transport modelling and measured concentrations by interpolation techniques, as well as meteorological and soil moisture inputs obtained from numerical models. By combining these modelled inputs with O_3 metric calculations and a survey of visible foliar O_3 injury in two ecologically important tree species, *F. sylvatica* and *P. abies*, this study provides a comprehensive overview of interannual patterns in O_3 phytotoxic potential expressed by both AOT40F and POD_1.

The *CL* for the exposure-based AOT40F index was set at 5 ppm·h. For flux-based assessment, the *CL* of POD_1 was defined as 5.2 mmol·m^{-2} PLA for *F. sylvatica* and 9.2 mmol·m^{-2} PLA for *P. abies* (CLRTAP 2024). In addition, Sicard et al. (2020) proposed a CL_{vis} of 12 mmol·m^{-2} POD_1 for broad-leaved species and 5 mmol·m^{-2} POD_1 for coniferous species. All of these *CL*s were exceeded at most monitored plots during the 2021–2023 vegetation seasons, with the exception of POD_1 at one site in 2022. This indicates a persistent exposure of forest vegetation to potentially phytotoxic O_3 concentrations under current conditions in the Czech Republic.

The POD_1 values showed a significant positive relationship with altitude in all three vegetation seasons, indicating an increased risk of O_3 uptake at higher elevations. In contrast, AOT40F did not consistently exhibit such a relationship, highlighting fundamental differences between exposure-based and flux-based O_3 risk metrics.

Meteorological and environmental conditions were most favourable for stomatal O_3 uptake in 2021, whereas the highest O_3 concentrations were observed in 2023. Although there were no statistically significant interannual differences in POD_1, site-specific patterns and means indicate that stomatal O_3 fluxes tended to be highest in 2021. This suggests that enhanced O_3 uptake was driven primarily by favourable conditions for stomatal conductance rather than by O_3 concentrations alone. Air temperature, soil moisture, and the O_3 concentration were identified as the most important factors controlling POD_1 variability.

Despite frequent exceedance of POD_1 *CL*s, only *F. sylvatica* presented visible foliar O_3 injury; no symptoms were detected in *P. abies*. In *F. sylvatica*, visible foliar O_3 injury occurred in two of the three vegetation seasons (2022 and 2023) and was spatially restricted, recorded at four out of eight plots. The relationship between visible foliar injury and O_3 indices was generally weak when all sites were considered. Nevertheless, the graphical patterns suggest a slightly stronger positive association between visible foliar O_3 injury and POD_1 than with AOT40F, for which there was no clear relationship.

Overall, the results support concerns that current exposure-based regulatory metrics may not adequately represent actual O_3 impacts on forest vegetation. These results further underline the relevance of flux-based approaches for O_3 risk assessment, particularly in heterogeneous environments. In addition, the interpretation of O_3 impacts based solely on visible O_3 foliar injury should be treated with caution under Czech conditions, as the results indicate substantial plot variability, even under comparable levels of O_3 uptake.

REFERENCES

Agathokleous E., Belz R.G., Calatayud V., De Marco A., Hoshika Y., Kitao M., Saitanis C.J., Sicard P., Paoletti E., Calabrese E.J. (2019): Predicting the effect of ozone on vegetation via linear non-threshold (LNT), threshold and hormetic dose-response models. Science of the Total Environment, 649: 61–74.

Agathokleous E., Feng Z., Oksanen E., Sicard P., Wang Q., Saitanis C.J., Araminiene V., Blande J.D., Hayes F., Calatayud V., Domingos M., Veresoglou S.D., Peñuelas J., Wardle D.A., De Marco A., Li Z., Harmens H., Yuan X., Vitale M., Paoletti E. (2020): Ozone affects plant, insect, and soil microbial communities: A threat to terrestrial ecosystems and biodiversity. Science Advances, 6: 1–17.

Agyei T., Juráň S., Ofori-Amanfo K.K., Šigut L., Urban O., Marek M.V. (2020): The impact of drought on total ozone flux in a mountain Norway spruce forest. Journal of Forest Science, 66: 280–278.

Ainsworth E.A. (2016): Understanding and improving global crop response to ozone pollution. The Plant Journal, 90: 886–897.

Anav A., De Marco A., Proietti C., Alessandri A., Dell'Aquila A., Cionni I., Friedlingstein P., Khvorostyanov D., Menut L., Paoletti E., Sicard P., Sitch S., Vitale M. (2016): Comparing concentration-based (AOT40) and stomatal uptake (PODY) metrics for ozone risk assessment to European forests. Global Change Biology, 22: 1608–1627.

Anav A., De Marco A., Collalti A., Emberson L., Feng Z., Lombardozzi D., Sicard P., Verbeke T., Viovy N., Vitale M., Paoletti E. (2022): Legislative and functional aspects of different metrics used for ozone risk assessment to forests. Environmental Pollution, 295: 118690.

https://doi.org/10.17221/24/2026-JFS

Araminienė V., Sicard P., Anav A., Agathokleous E., Stakėnas V., De Marco A., Varnagirytė-Kabašinskienė I., Paoletti E., Girgždienė R. (2019): Trends and interrelationships of ground-level ozone metrics and forest health in Lithuania. Science of The Total Environment, 666: 1265 1277.

Ashmore M.R. (2005): Assessing the future global impacts of ozone on vegetation. Plant, Cell and Environment, 28: 949–964.

Bergmann E., Bender J., Weigel H.J. (1999): Ozone threshold doses and exposure–response relationships for the development of ozone injury symptoms in wild plant species. New Phytologist, 144: 423–435.

Bergmann E., Bender J., Weigel H.J. (2017): Impact of tropospheric ozone on terrestrial biodiversity: A literature analysis to identify ozone sensitive taxa. Journal of Applied Botany and Food Quality, 90: 83–105.

Bičárová S., Sitková Z., Pavlendová H. (2016): Ozone phytotoxicity in the Western Carpathian Mountains in Slovakia. Forestry Journal, 62: 77–88.

Bičárová S., Sitková Z., Pavlendová H., Fleischer Jr P., Fleischer Sr P., Bytnerowicz A. (2019): The role of environmental factors in ozone uptake of *Pinus mugo* Turra. Atmospheric Pollution Research, 10: 283–293.

Bičárová S., Shashikumar A., Dalstein-Richier L., Lukasová V., Adamčíková K., Pavlendová H., Sitková Z., Buchholcerová A., Bilčík D. (2020): The response of *Pinus* species to ozone uptake in different climate regions of Europe. Central European Forestry Journal, 66: 255–268.

Boháčová L., Lomský B., Šrámek V. (2011): Development of the Monitoring of Forest Health State Under Life+ 'FutMon' Project in the Czech Republic. Strnady, Forestry and Game Management Research Institute: 58. Available at: https://invenio.nusl.cz/record/432014/files/nusl-432014_1.pdf

Breiman L. (2001): Random forests. Machine Learning, 45: 5–32.

Brodin M., Helmig D., Oltmans S.J. (2010): Seasonal ozone behavior along an elevation gradient in the Colorado Front Range Mountains. Atmospheric Environment, 44: 5305–5315.

Büker P., Morrissey T., Briolat A., Falk R., Simpson D., Tuovinen J.P., Alonso R., Barth S., Baumgarten M., Grulke N., Karlsson P.E., King J., Lagergren F., Matyssek R., Nunn A., Ogaya R., Peñuelas J., Rhea L., Schaub M., Uddling J., Werner W., Emberson L.D. (2012): DO3SE modelling of soil moisture to determine ozone flux to forest trees. Atmospheric Chemistry and Physics, 12: 5537–5562.

Burkey K.O., Wei C., Eason G., Ghosh P., Fenner G.P. (2000): Antioxidant metabolite levels in ozone-sensitive and tolerant genotypes of snap bean. Physiologia Plantarum, 110: 195–200.

Burley J.D., Bytnerowicz A. (2011): Surface ozone in the White Mountains of California. Atmospheric Environment, 45: 4591–4602.

Carrari E., Dalstein L., Hoshika Y., Paoletti E. (2020): MOTTLES atlas of visible foliar ozone injury. Available at: https://mottles-project.wixsite.com/life/atlas-ozone-injury

CLRTAP (2017): Chapter III: Mapping critical levels for vegetation. In: Manual on Methodologies and Criteria for Modelling and Mapping Critical Loads and Levels and Air Pollution Effects, Risks, and Trends. UNECE Convention on Long Range Transboundary Air Pollution: 66. Available at: https://icpvegetation.ceh.ac.uk/sites/default/files/FinalnewChapter3v4Oct2017_000.pdf

CLRTAP (2020): Scientific Background Document B of Chapter 3 of 'Manual on Methodologies and Criteria for Modelling and Mapping Critical Loads and Levels and Air Pollution Effects, Risks, and Trends'. UNECE Convention on Long Range Transboundary Air Pollution: 108. Available at: https://icpvegetation.ceh.ac.uk/sites/default/files/Scientific%20Background%20document%20B%20June%202020.pdf

CLRTAP (2024): Chapter III: Mapping critical levels for vegetation and lichens. In: Manual on Methodologies and Criteria for Modelling and Mapping Critical Loads and Levels and Air Pollution Effects, Risks, and Trends. Update 2024. UNECE Convention on Long Range Transboundary Air Pollution: 68–137. Available at: https://www.umweltbundesamt.de/sites/default/files/medien/11850/publikationen/123_2024_texte_manual_on_methodologies_and_criteria.pdf

Coates J., Mar K.A., Ojha N., Butler T.M. (2016): The influence of temperature on ozone production under varying NO_X conditions – A modelling study. Atmospheric Chemistry and Physics, 16: 11601–11615.

Coulston J.W., Smith G.C., Smith W.D. (2003): Regional assessment of ozone sensitive tree species using bioindicator plants. Environmental Monitoring and Assessment, 83: 113–127.

Dalstein L., Ciriani M.L. (2019): Ozone foliar damage and defoliation monitoring of *P. cembra* between 2000 and 2016 in the southeast of France. Environmental Pollution, 244: 451–461.

De Marco A., Proietti C., Anav A., Ciancarella L., D'Elia I., Fares S., Fornasier M.F., Fusaro L., Gualtieri M., Manes F., Marchetto A., Mircea M., Paoletti E., Piersanti A., Rogora M., Salvati L., Salvatori E., Screpanti A., Vialetto G., Vitale M., Leonardi C. (2019): Impacts of air pollution on human and ecosystem health, and implications for the National Emission Ceilings Directive: Insights from Italy. Environment International, 125: 320–333.

https://doi.org/10.17221/24/2026-JFS

Díaz-de-Quijano M., Peñuelas J., Ribas À. (2009): Increasing interannual and altitudinal ozone mixing ratios in the Catalan Pyrenees. Atmospheric Environment, 43: 6049–6057.

Dumont J., Spicher F., Montpied P., Dizengremel P., Jolivet Y., Le Thiec D. (2013): Effects of ozone on stomatal responses to environmental parameters (blue light, red light, CO_2 and vapour pressure deficit) in three *Populus deltoides* × *Populus nigra* genotypes. Environmental Pollution, 173: 85–96.

EC (2008): Directive 2008/50/EC of the European Parliament and of the Council of 21 May 2008 on ambient air quality and cleaner air for Europe. European Parliament, Council of the European Union. Available at: https://eur-lex.europa.eu/legal-content/EN/TXT/?uri=CELEX%3A32008L0050

Eghdami H., Werner W., Büker P., Sicard P. (2022): Assessment of ozone risk to Central European forests: Time series indicates perennial exceedance of ozone critical levels. Environmental Research, 203: 111798.

Emberson L.D., Ashmore M.R., Cambridge H.M., Simpson D., Tuovinen J.P. (2000): Modelling stomatal ozone flux across Europe. Environmental Pollution, 109: 403–413.

EU (2016): Directive (EU) 2016/2284 of the European Parliament and of the Council of 14 December 2016 on the reduction of national emissions of certain atmospheric pollutants, amending Directive 2003/35/EC and repealing Directive 2001/81/EC. European Parliament, Council of the European Union. Available at: https://eur-lex.europa.eu/eli/dir/2016/2284

EU (2019): Communication from the Commission — Commission Notice on ecosystem monitoring under Article 9 and Annex V of Directive (EU) 2016/2284 of the European Parliament and of the Council on the reduction of national emissions of certain atmospheric pollutants (NEC-Directive). European Parliament, Council of the European Union. Available at: https://eur-lex.europa.eu/legal-content/EN/TXT/?uri=oj:JOC_2019_092_R_0001

EU (2024): Directive (EU) 2024/2881 of the European Parliament and of the Council of 23 October 2024 on ambient air quality and cleaner air for Europe (recast). European Parliament, Council of the European Union. Available at: https://eur-lex.europa.eu/eli/dir/2024/2881/oj/eng

Fares S., McKay M., Holzinger R., Goldstein A.H. (2010): Ozone fluxes in a *Pinus ponderosa* ecosystem are dominated by non-stomatal processes: Evidence from long-term continuous measurements. Agricultural and Forest Meteorology, 150: 420–431.

Fares S., Conte A., Chabbi A. (2018): Ozone flux in plant ecosystems: New opportunities for long-term monitoring networks to deliver ozone-risk assessments. Environmental Science and Pollution Research, 25: 8240–8248.

Finlayson-Pitts B.J., Pitts Jr J.N. (2000): Chemistry of the Upper and Lower Atmosphere. San Diego, Academic Press: 969.

Fowler D., Amann M., Anderson R., Ashmore M., Cox P., Depledge M., Derwent D., Grennfelt P., Hewitt N.,Hov O., Jenkin M., Kelly F., Liss P., Pilling M., Pyle J., Slingo J., Stevenson D. (2008): Ground-Level Ozone in the 21st Century: Future Trends, Impacts and Policy Implications. RS Policy Document 15/08. London, The Royal Society: 131.

Fuhrer J. (2002): Ozone impacts on vegetation. Ozone: Science& Engineering, 24: 69–74.

Horálek J., Vlasáková L., Schreiberová M., Benešová N., Schneider P., Kurfürst P., Tognet F., Vlček O., Školoudová L. (2025): Air quality maps of EEA member and cooperating countries for 2023. PM_{10}, $PM_{2.5}$, O_3, NO_2, NOx and BaP spatial estimates and their uncertainties (Eionet Report – ETC HE 2025/5). European Topic Centre on Human Health and the Environment: 143. Available at: https://zenodo.org/records/17427294

Hoshika Y., Carrari E., Mariotti B., Martini S., De Marco A., Sicard P., Paoletti E. (2020): Flux-based ozone risk assessment for a plant injury index (PII) in three European cool-temperate deciduous tree species. Forests, 11: 82.

Hůnová I., Matoušková L., Srněnský R., Koželková K. (2011): Ozone influence on native vegetation in the Jizerske hory Mts. of the Czech Republic: Results based on ozone exposure and ozone-induced visible symptoms. Environmental Monitoring and Assessment, 183: 501–515.

Huttunen S., Manninen S. (2013): A review of ozone responses in Scots pine (*Pinus sylvestris*). Environmental and Experimental Botany, 90: 17–31.

Innes J.L., Skelly J.M., Schaub M. (2001): Ozone and Broadleaved Species: A Guide to the Identification of Ozone induced Foliar Injury. Bern, Haupt: 136.

Jones M.E., Paine T.D., Fenn M.E., Poth M.A. (2004): Influence of ozone and nitrogen deposition on bark beetle activity under drought conditions. Forest Ecology and Management, 200: 67–76.

JRC (2016): Maps of indicators of soil hydraulic properties for Europe. [Dataset]. European Soil Data Centre. Available at: https://esdac.jrc.ec.europa.eu

Karlsson P.E., Klingberg J., Engardt M., Andersson C., Langner J., Pihl Karlsson G., Pleijel H. (2017): Past, present and future concentrations of ground-level ozone and potential impacts on ecosystems and human health in northern Europe. Science of the Total Environment, 576: 22–35.

Karlsson P.E., Büker P., Bland S., Simpson D., Sharps K., Hayes F., Emberson L.D. (2025): Ozone causes substantial reductions in the carbon sequestration of managed European forests. Biogeosciences, 22: 3563–3582.

Kodrík J., Kodrík M. (2002): Root biomass of beech as a factor influencing the wind tree stability. Journal of Forest Science, 48: 549–564.

https://doi.org/10.17221/24/2026-JFS

Koltay A. (2025): The effect of ozone in Hungarian forests. In: Influence of Air Pollution and Climate Change on Forest Dynamics: Programme and Abstracts, Split, Sept 1–5, 2025: 96.

Langebartels C., Heller W., Führer G., Lippert M., Simons S., Sandermann Jr H. (1998): Memory effects in the action of ozone on conifers. Ecotoxicology and Environmental Safety, 41: 62–72.

Lukasová V., Varšová S., Žatková L., Adamčíková K., Buchholcerová A., Onderka M., Milovský R., Bilčík D., Mináriková V. (2025): Indication of the sensitivity of *Pinaceae* species growing in Eastern Central Europe to ground-level ozone pollution. Environmental Science and Pollution Research, 32: 2638–2655.

Marra E., De Marco A., Ebone A., Ferrara A.M., Giannetti F., Tagliaferro F., Sicard P., Andrei A. (2025): Flux-based assessment of ozone visible foliar injury in the Southern Alps. Journal of Forestry Research, 36: 124.

Manning W.J., Godzik B. (2004): Bioindicator plants for ambient ozone in Central and Eastern Europe. Environmental Pollution, 130: 33–39.

Manzini J., Hoshika Y., Moura B.B., Paoletti E. (2023): Exploring a new O_3 index as a proxy for the avoidance/tolerance capacity of forest species to tolerate O_3 injury. Forests, 14: 901.

Matyssek R., Wieser G., Nunn A.J., Kozovits A.R., Reiter I.M., Heerdt C., Winkler J.B., Baumgarten M., Häberle K.H., Grams T.E.E., Werner H., Fabian P., Havranek W.M. (2004): Comparison between AOT40 and ozone uptake in forest trees of different species, age and site conditions. Atmospheric Environment, 38: 2271–2281.

Matyssek R., Bytnerowicz A., Karlsson P.E., Paoletti E., Sanz M., Schaub M., Wieser G. (2007): Promoting the ozone flux concept for European forest trees. Environmental Pollution, 146, 587–607.

Medlyn B.E., Barton C.V.M., Broadmeadow M.S.J., Ceulemans R., De Angelis P., Forstreuter M., Freeman M., Jackson S.B., Kellomäki S., Laitat E., Rey A., Roberntz P., Sigurdsson B.D., Strassemeyer J., Wang K., Curtis P.S., Jarvis P.G. (2001): Stomatal conductance of forest species after long-term exposure to elevated CO_2 concentration: A synthesis. New Phytologist, 149: 247–264.

Mills G., Pleijel H., Braun S., Büker P., Bermejo V., Calvo E., Danielsson H., Emberson L., González Fernández I., Grünhage L., Harmens H., Hayes F., Karlsson P.E., Simpson D. (2011): New stomatal flux-based critical levels for ozone effects on vegetation. Atmospheric Environment, 45: 5064–5068.

Mills G., Pleijel H., Malley C.S., Sinha B., Cooper O.R., Schultz M.G., Neufeld H.S., Simpson D., Sharps K., Feng Z., Gerosa G., Harmens H., Kobayashi K., Saxena P., Paoletti E., Sinha V., Xu X. (2018): Tropospheric Ozone Assessment Report: Present-day tropospheric ozone distribution and trends relevant to vegetation. Elementa: Science of the Anthropocene, 6: 47.

Monks P.S., Archibald A.T., Colette A., Cooper O., Coyle M., Derwent R., Fowler D., Granier C., Law K.S., Mills G.E., Stevenson D.S., Tarasova O., Thouret V., von Schneidemesser E., Sommariva R., Wild O., Williams M.L. (2015): Tropospheric ozone and its precursors from the urban to the global scale: From air quality to short-lived climate forcer. Atmospheric Chemistry and Physics, 15: 8889–8973.

Muñoz-Sabater J. (2019). ERA5-Land hourly data from 1950 to present. Arctic Data Center. Available at: https://arctic-data.io/catalog/view/doi:10.18739/A2C24QQ0W

Musselman R.C., Massman W.J. (1999): Ozone flux to vegetation and its relationship to plant response and ambient air quality standards. Atmospheric Environment, 33: 65–73.

MoA (2025): Zpráva o stavu lesa a lesního hospodářství České republiky v roce 2024. 1st Ed. Prague, Ministry of Agriculture of the Czech Republic: 128. (in Czech)

Novotný R., Buriánek V., Šrámek V. (2009): Metodika hodnocení viditelného poškození vegetace vyvolaného účinky přízemního ozonu. Lesnický průvodce 6. Strnady, Forestry and Game Management Research Institute: 48. Available at: https://www.vulhm.cz/files/uploads/2019/03/lp_2009_06.pdf (in Czech)

Novotný R., Šrámek V., Buriánek V. (2010): Evaluation of the ozone injury to ground vegetation within the plots of intensive monitoring in the Czech Republic. Lesnícky časopis – Forestry Journal, 56: 57–67. Available at: https://scispace.com/pdf/evaluation-of-the-ozone-injury-to-ground-vegetation-within-1o7dbzd5b2.pdf

Nunn A.J., Reiter I.M., Häberle K.H., Werner H., Langebartels C., Sandermann H., Heerdt C., Fabian P., Matyssek R. (2002): 'Free-air' ozone canopy fumigation in an old-growth mixed forest: Concept and observations in beech. Phyton, 42: 105–119.

Nunn A.J., Kozovits A.R., Reiter I.M., Heerdt C., Leuchner M., Lütz C., Liu X., Löw M., Winkler J.B., Grams T.E.E., Häberle K.H., Werner H., Fabian P., Rennenberg H., Matyssek R. (2005): Comparison of ozone uptake and sensitivity between a phytotron study with young beech and a field experiment with adult beech (*Fagus sylvatica*). Environmental Pollution, 137: 494–506.

Nussbaum S., Remund J., Rihm B., Mieglitz K., Gurtz J., Fuhrer J. (2003): High-resolution spatial analysis of stomatal ozone uptake in arable crops and pastures. Environment International, 29: 385–392.

Oravcová Z., Vido J. (2022): Understanding the complexity of drought within the soil profile in beech ecosystems on their lower altitudinal limit in Slovakia. Water, 14: 1338.

https://doi.org/10.17221/24/2026-JFS

Paoletti E. (2006): Impact of ozone on Mediterranean forests: A review. Environmental Pollution, 144: 463–474.

Paoletti E., Manning W. (2007): Toward a biologically significant and usable standard for ozone that will also protect plants. Environmental Pollution, 150: 85–95.

Paoletti E., Alivernini A., Anav A., Badea O., Carrari E., Chivulescu S., Conte A., Ciriani M.L., Dalstein-Richier L., De Marco A., Fares S., Fasano G., Giovannelli A., Lazzara M., Leca S., Materassi A., Moretti V., Pitar D., Popa I., Sabatini F., Salvati L., Sicard P., Sorgi T., Hoshika Y. (2019): Toward stomatal–flux based forest protection against ozone: The MOTTLES approach. Science of the Total Environment, 691: 516–527.

Paoletti E., Sicard P., Hoshika Y., Fares S., Badea O., Pitar D., Popa I., Anav A., Moura B.B., De Marco A. (2022): Towards long-term sustainability of stomatal ozone flux monitoring at forest sites. Sustainable Horizons, 2: 100018.

Pell E.J., Schlagnhaufer C.D., Arteca R.N. (1997): Ozone induced oxidative stress: Mechanisms of action and reaction. Physiologia Plantarum, 100: 264–273.

R Core Team (2024): R: A language and environment for statistical computing. Vienna, R Foundation for Statistical Computing. Available at: https://www.R-project.org/

Ramboll US Consulting (2018): User's Guide: Comprehensive Air Quality Model with Extensions (CAMx). Version 6.50. Novato, Ramboll Environment and Health: 284. Available at: https://www.camx.com/Files/CAMxUsersGuide_v6.50.pdf

Reif J., Gamero A., Flosek J., Hůnová I. (2023): Ambient ozone – New threat to birds in mountain ecosystems? Science of the Total Environment, 876: 162711.

Ronan A.C., Ducker J.A., Schnell J.L., Holmes C.D. (2020): Have improvements in ozone air quality reduced ozone uptake into plants? Elementa: Science of the Anthropocene, 8: 2.

Schaub M., Calatayud V. (2013): Assessment of visible foliar injury induced by ozone. Developments in Environmental Science, 12: 205–221.

Schaub M., Calatayud V., Ferretti M., Brunialti G., Lövblad G., Krause G., Sanz M.J., Pitar D., Gottardini E. (2020): Part VIII: Assessment of ozone injury. Version 2020-1. In: UNECE ICP Forests Programme Co-ordinating Centre (ed.): Manual on Methods and Criteria for Harmonized Sampling, Assessment, Monitoring and Analysis of the Effects of Air Pollution on Forests. Eberswalde, Thünen Institute of Forest Ecosystems: 15 + Annex.

Schmid I. (2002): The influence of soil type and interspecific competition on the fine root system of Norway spruce and European beech. Basic and Applied Ecology, 3: 339–346.

Seinfeld J.H., Pandis S.N. (2006): Atmospheric Chemistry and Physics: From Air Pollution to Climate Change. 2nd Ed. New York, John Wiley & Sons: 1152.

Sicard P., De Marco A., Dalstein-Richier L., Tagliaferro F., Renou C., Paoletti E. (2016a): An epidemiological assessment of stomatal ozone flux-based critical levels for visible ozone injury in Southern European forests. Science of the Total Environment, 541: 729–741.

Sicard P., Augustaitis A., Belyazid S., Calfapietra C., De Marco A., Fenn M., Bytnerowicz A., Grulke N., He S., Matyssek R., Serengil Y., Wieser G., Paoletti E. (2016b): Global topics and novel approaches in the study of air pollution, climate change and forest ecosystems. Environmental Pollution, 213: 977–987.

Sicard P., Anav A., De Marco A., Paoletti E. (2017): Projected global ground-level ozone impacts on vegetation under different emission and climate scenarios. Atmospheric Chemistry and Physics, 17: 12177–12196.

Sicard P., De Marco A., Carrari E., Dalstein-Richier L., Hoshika Y., Badea O., Pitar D., Fares S., Conte A., Popa I., Paoletti E. (2020): Epidemiological derivation of flux-based critical levels for visible ozone injury in European forests. Journal of Forestry Research, 31: 1509–1519.

Sicard P., Hoshika Y., Carrari E., De Marco A., Paoletti E. (2021): Testing visible ozone injury within a light exposed sampling site as a proxy for ozone risk assessment for European forests. Journal of Forestry Research, 32: 1351–1359.

Simpson D., Benedictow A., Berge H., Bergström R., Emberson L.D., Fagerli H., Flechard C.R., Hayman G.D., Gauss M., Jonson J.E., Jenkin M.E., Nyíri A., Richter C., Semeena V.S., Tsyro S., Tuovinen J.P., Valdebenito Á., Wind P. (2012): The EMEP MSC-W chemical transport model – Technical description. Atmospheric Chemistry and Physics, 12: 7825–7865.

Skärby L., Ro-Poulsen H., Wellburn F.A.M., Sheppard L.J. (1998): Impacts of ozone on forests: |A European perspective. New Phytologist, 139: 109–122.

Smidt S., Herman F. (2004): Evaluation of air pollution-related risks for Austrian mountain forests. Environmental Pollution, 130: 99–112.

Šrámek V., Novotný R., Vejpustková M., Hůnová I., Uhlířová H. (2012): Monitoring of ozone effects on the vitality and increment of Norway spruce and European beech in the Central European forests. Journal of Environmental Monitoring, 14: 1696–1702.

Termonia P., Fischer C., Bazile E., Bouyssel F., Brožková R., Bénard P., Bochenek B., Degrauwe D., Derková M., El Khatib R., Hamdi R., Mašek J., Pottier P., Pristov N., Seity Y., Smolíková P., Španiel O., Tudor M., Wang Y., Wittmann C., Joly A. (2018): The ALADIN system and its canonical model configurations AROME CY41T1 and ALARO CY40T1. Geoscientific Model Development, 11: 257–281.

https://doi.org/10.17221/24/2026-JFS

Vacek S., Balcar V. (2004): Sustainable management of mountain forests in the Czech Republic. Journal of Forest Science, 50: 526–532.

Vacek Z., Tomášková I., Fuchs Z., Šimůnek V., Vacek S., Cukor J., Bílek L., Gallo J., Zlatuška K., Duchan M. (2025): Impact of technical water retention on European beech (*Fagus sylvatica* L.) resilience and growth dynamics. Journal of Forest Science, 71: 124–137.

Viviano A., Tanaka R., Paoletti E., Marra E., Moura B.B., Manzini J., Hoshika Y. (2025): Stomatal ozone flux estimation in Mediterranean forests through sap flow analysis. Journal of Environmental Sciences, 165: 516–525.

Vlasáková-Matoušková L., Hůnová I. (2015): Stomatal ozone flux and visible leaf injury in native juvenile trees of *Fagus sylvatica* L.: A field study from the Jizerské hory Mts., the Czech Republic. Environmental Science and Pollution Research, 22: 10034–10046.

Vollenweider P., Ottiger M., Günthardt-Goerg M.S. (2003): Validation of leaf ozone symptoms in natural vegetation using microscopical methods. Environmental Pollution, 124: 101–118.

Wieser G., Häsler R., Götz B., Koch W., Havranek W.M. (2000): Role of climate, crown position, tree age, and altitude in calculated ozone flux into needles of *Picea abies* and *Pinus cembra*: A synthesis. Environmental Pollution, 109: 415–422.

Withington J.M., Reich P.B., Oleksyn J., Eissenstat D.M. (2006): Comparisons of structure and life span in roots and leaves among temperate trees. Ecological Monographs, 76: 381–397.

Zapletal M., Pretel J., Chroust P., Cudlín P., Edwards-Jonášová M., Urban O., Pokorný R., Czerný R., Hůnová I. (2012): The influence of climate change on stomatal ozone flux to a mountain Norway spruce forest. Environmental Pollution, 169: 267–273.

Zapletal M., Juráň S., Krpeš V., Michna K., Edwards-Jonášová M., Cudlín P. (2018): Effect of ozone flux on selected structural and antioxidant characteristics of a mountain Norway spruce forest. Baltic Forestry, 24: 261–267.

Zhang X., Lyu J., Han Y., Sun N., Sun W., Li J., Liu C., Yin S. (2020): Effects of the leaf functional traits of coniferous and broadleaved trees in subtropical monsoon regions on PM2.5 dry deposition velocities. Environmental Pollution, 265: 114845.

Received: March 9, 2026
Accepted: April 27, 2026
Published online: May 21, 2026